Supplementary Information

Phase-interface-anchored cadmium single-atom catalysts for efficient methanol steam reforming

Shunan Zhang[1], Haozhi Zhou[1], Zilong Shao[2], Baohuan Wei[3], Zhen Hu[3], Hao Liang[1], Ruonan Zhang[1], Xiaofang Liu[2], Hu Luo[2], Lin Xia[2], Yuhan Sun[1,3], Hui Wang[1,2]*

[1] Institute of Carbon Neutrality, ShanghaiTech University, Shanghai 201203, PR China

[2] CAS Key Laboratory of Low-Carbon Conversion Science and Engineering, Shanghai Advanced Research Institute, Chinese Academy of Sciences, Shanghai 201210, PR China

[3] Shanghai Institute of Clean Technology, Shanghai 201620, P. R. China

*Corresponding author. Tel: +86-021-20608002, Fax: +86-021-20608066.

E-mail: wanghh@sari.ac.cn (H. Wang);

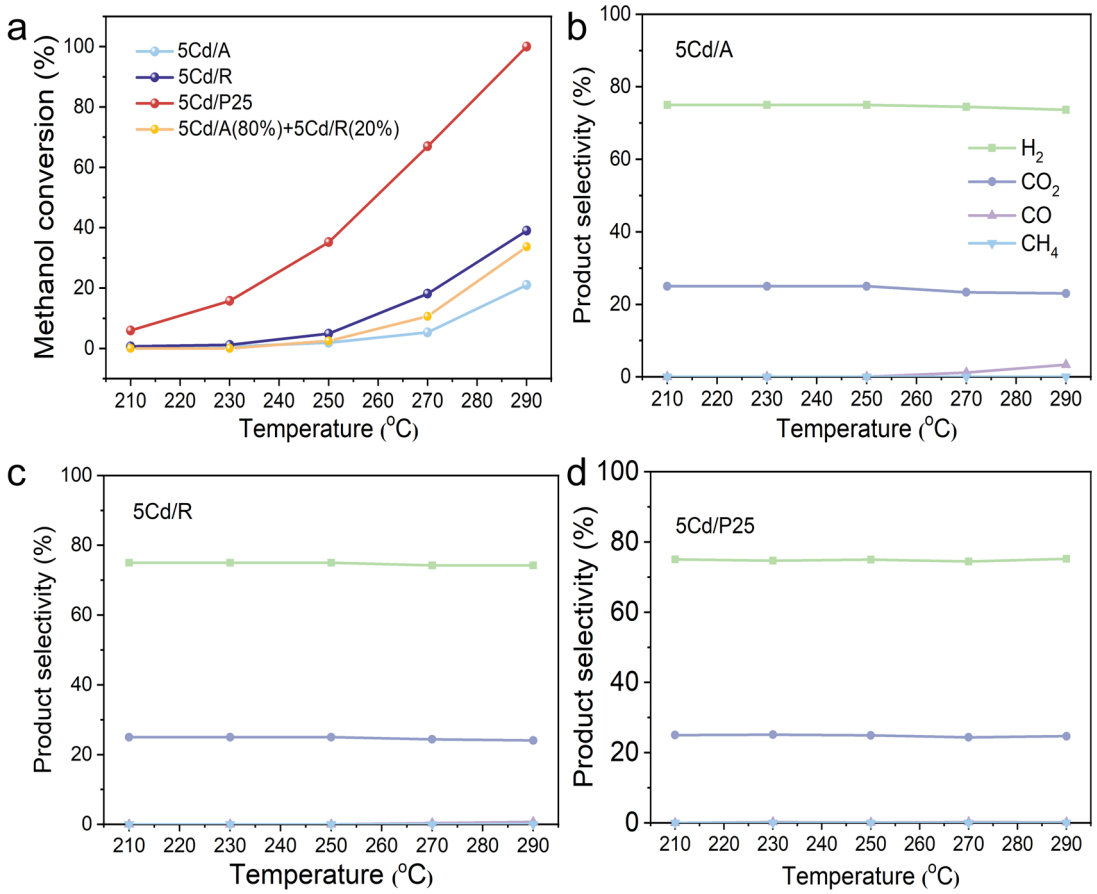

Fig. S1 Evolution of methanol conversion (**a**) and product selectivity in response to temperature increments for the 5Cd/A (**b**), 5Cd/R (**c**), and 5Cd/P25 (**d**) catalysts. Reaction conditions: 210-290°C, S/C ratio of 3/1, 0.1 MPa pressure, and 3 mL g^{-1} h^{-1} feed rate.

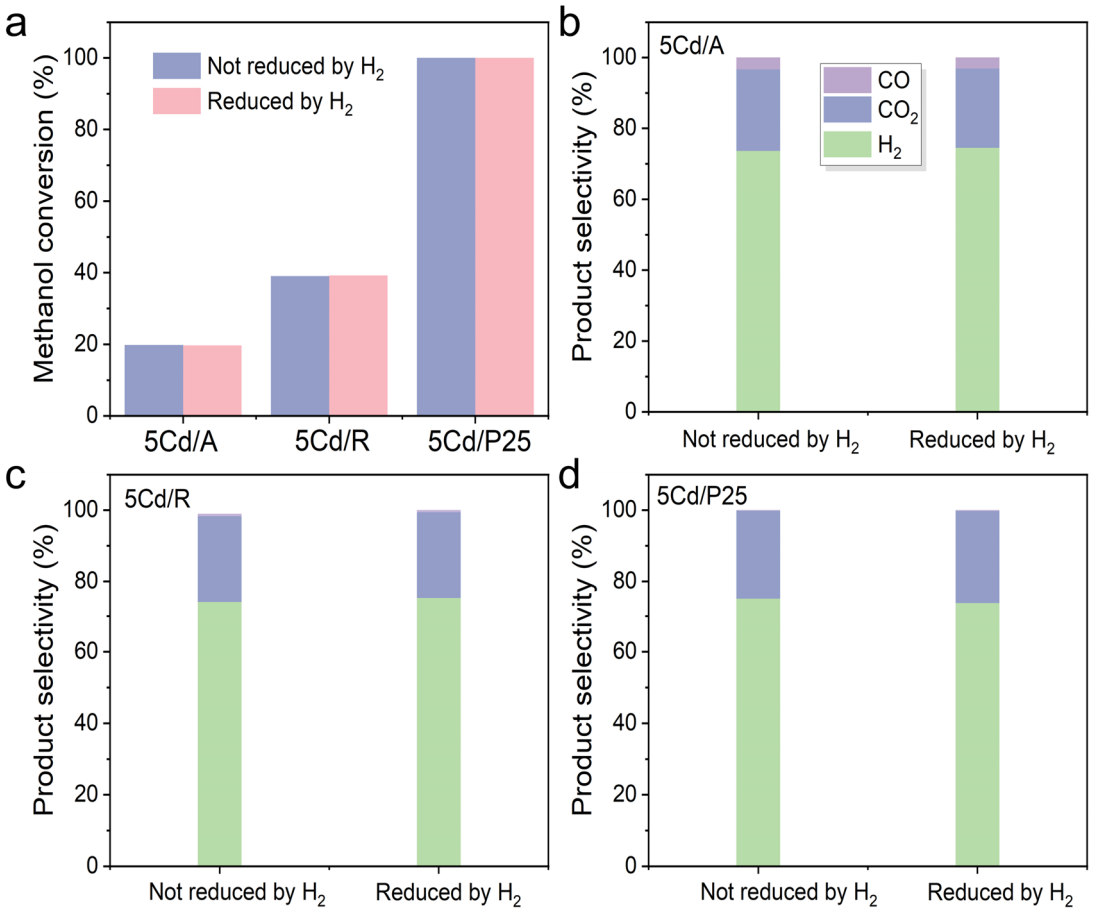

Fig. S2 Comparative analysis of methanol conversion and product selectivity pre- and post-H_2 reduction. Reduction conditions: 290℃, H_2 (50mL/min), and atmospheric pressure. Reaction conditions: 290℃, S/C ratio of 3/1, 0.1 MPa pressure, and 3 mL g^{-1} h^{-1} feed rate.

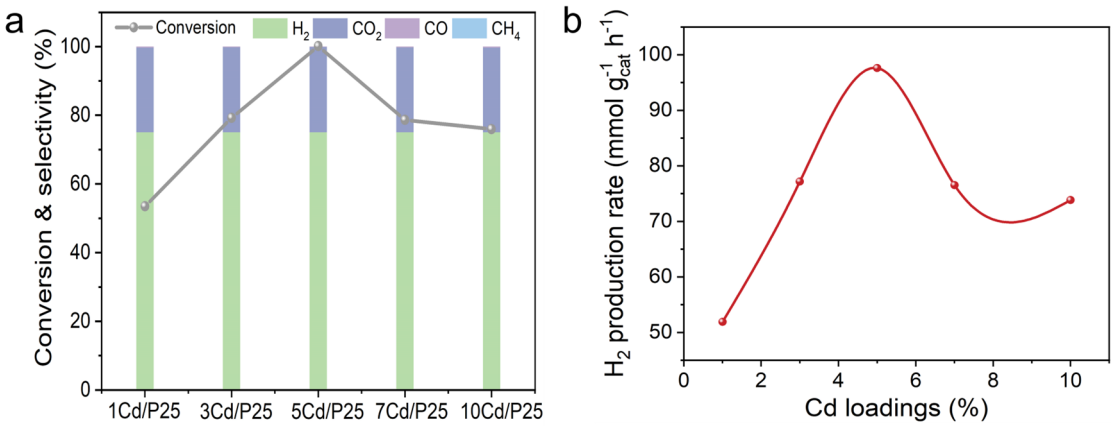

Fig. S3 Catalytic performance as a function of varying Cd loadings on the P25 support. Reaction conditions: 290°C, S/C ratio of 3/1, 0.1 MPa pressure, and 3 mL g^{-1} h^{-1} feed rate.

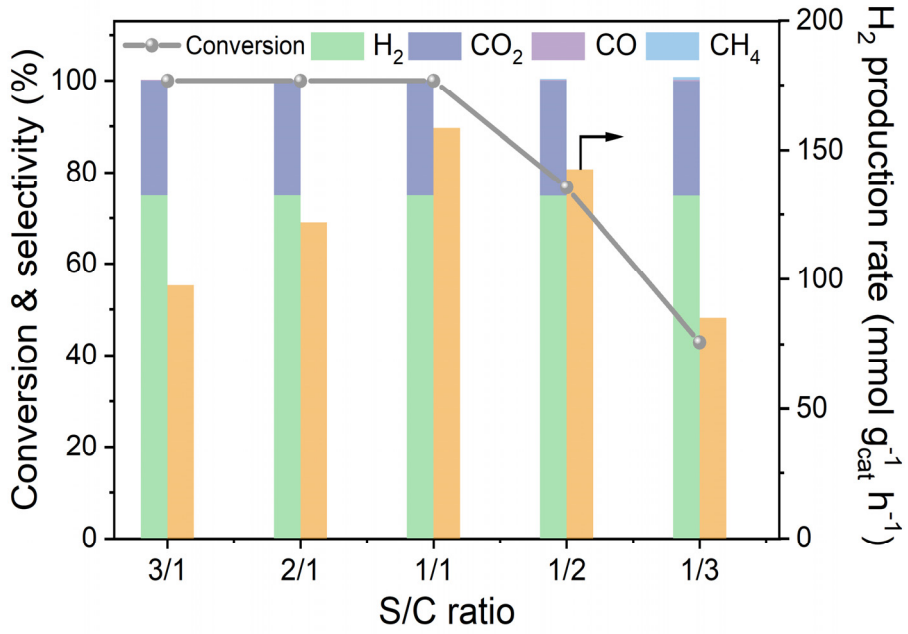

Fig. S4 Variation in catalytic performance of the 5Cd/P25 catalyst with respect to the S/C ratio. Reaction conditions: 290°C, 0.1 MPa pressure, and 3 mL g^{-1} h^{-1} feed rate.

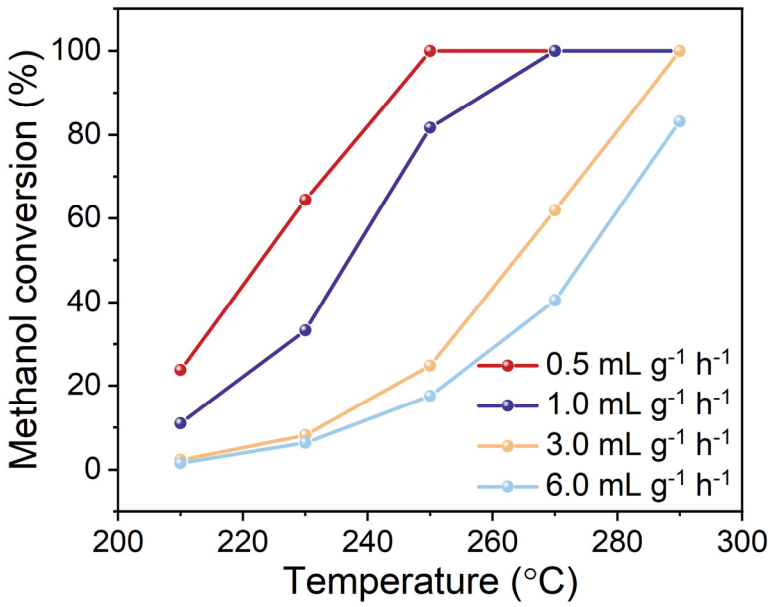

Fig. S5 Methanol conversion of the 5Cd/P25 catalyst at varying feed rates in conjunction with elevated temperatures. Reaction conditions: 210-290°C, S/C ratio of 1/1, 0.1 MPa pressure, and 0.5-6.0 mL g^{-1} h^{-1} feed rate.

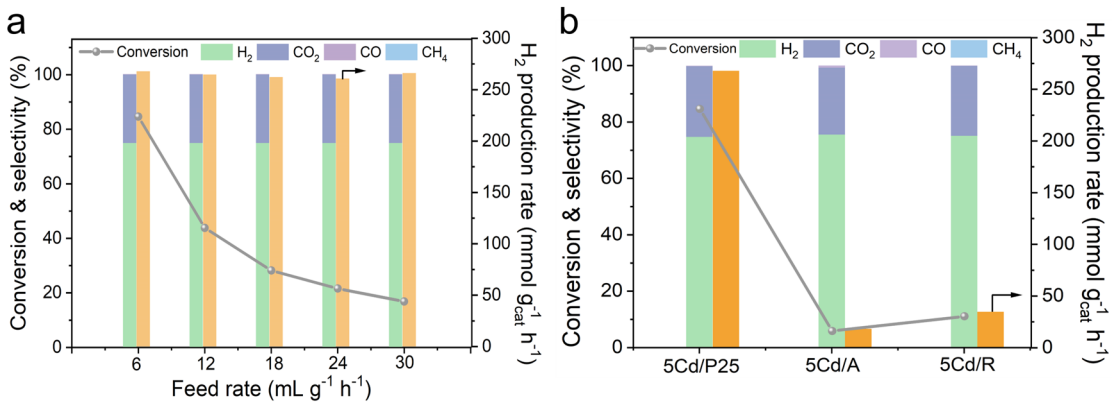

Fig. S6 (**a**) Catalytic performance changes of the 5Cd/P25 catalyst as a function of feed rate. Reaction conditions: 290℃, S/C ratio of 1/1, 0.1 MPa pressure, and 6-30 mL g^{-1} h^{-1} feed rate. (**b**) Catalytic performance of the 5Cd/P25, 5Cd/A, and 5Cd/R catalysts under the conditions of 290℃, S/C ratio of 1/1, 0.1 MPa pressure, and 6 mL g^{-1} h^{-1} feed rate.

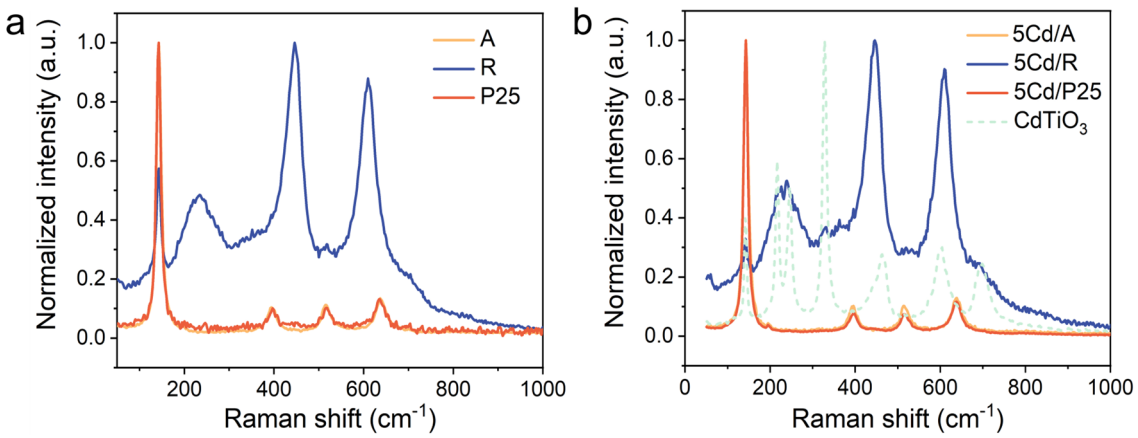

Fig. S7 Comparative Raman spectroscopy analysis of different support materials (**a**) and catalysts (**b**).

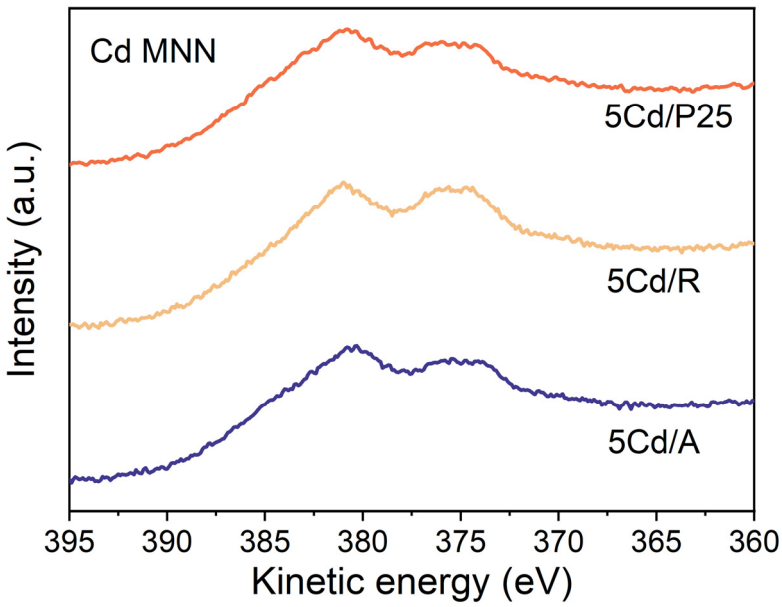

Fig. S8 AES results for the fresh 5Cd/A, 5Cd/R, and 5Cd/P25 catalysts.

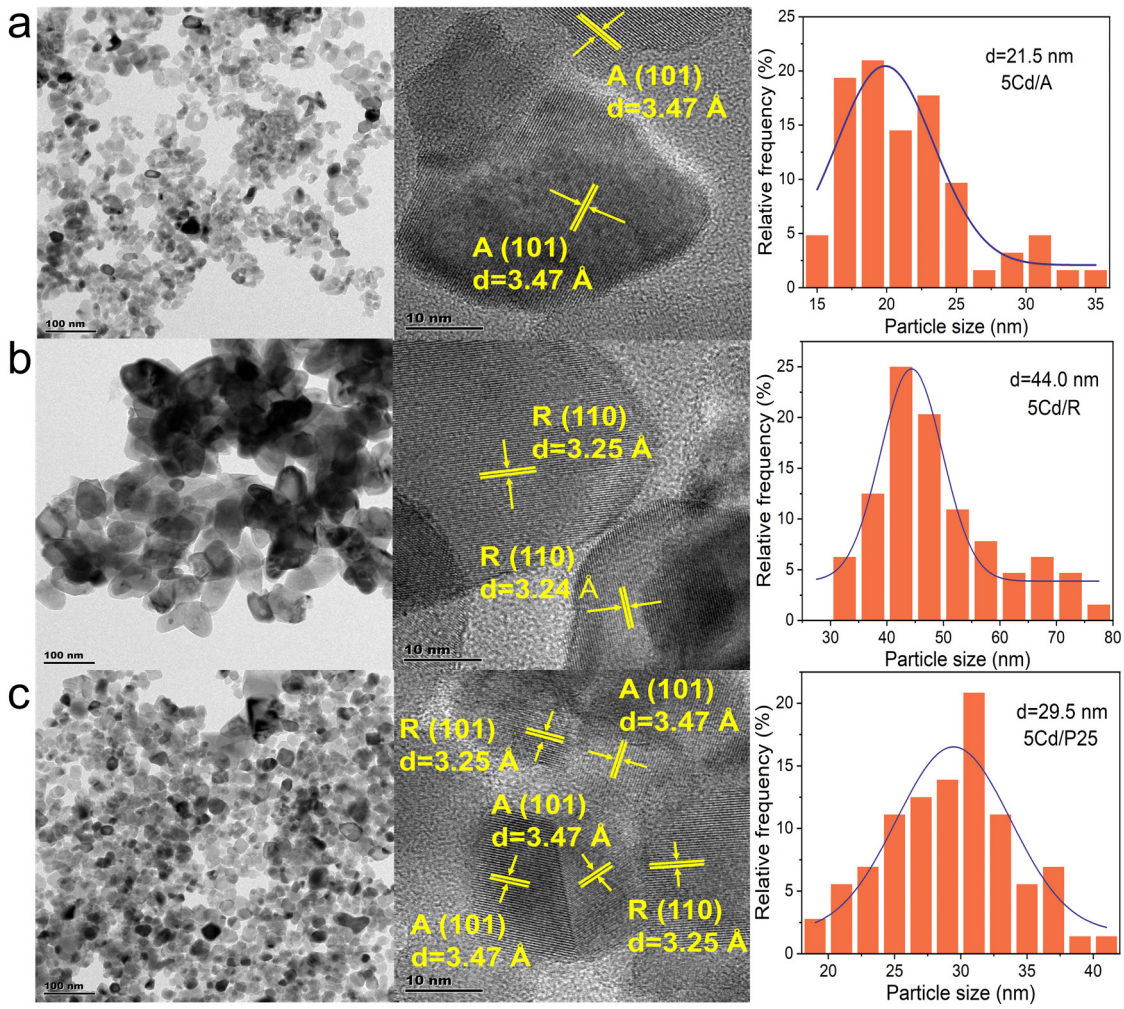

Fig. S9 TEM and HRTEM images alongside particle size distribution for three catalysts: (**a**) 5Cd/A; (**b**) 5Cd/R; (**c**) 5Cd/P25.

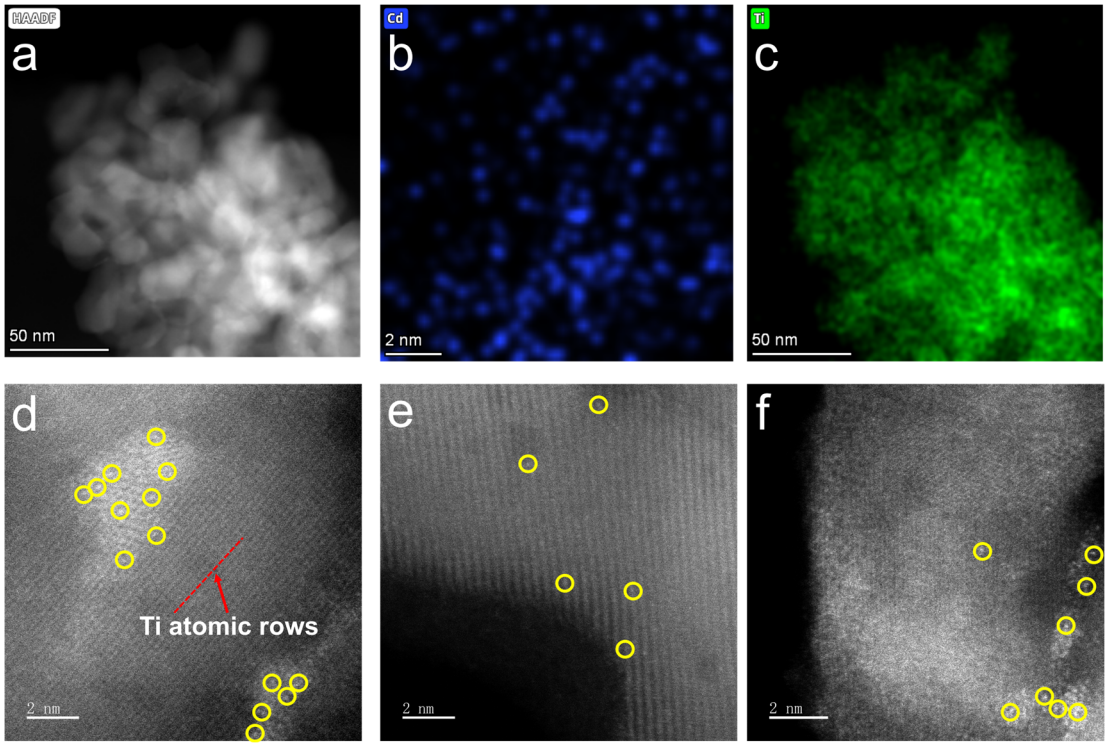

Fig. S10 EDX mapping (**a-c**) and HAADF-STEM (**d-f**) images of the 5Cd/A catalyst. (Cd single atoms were highlighted in yellow).

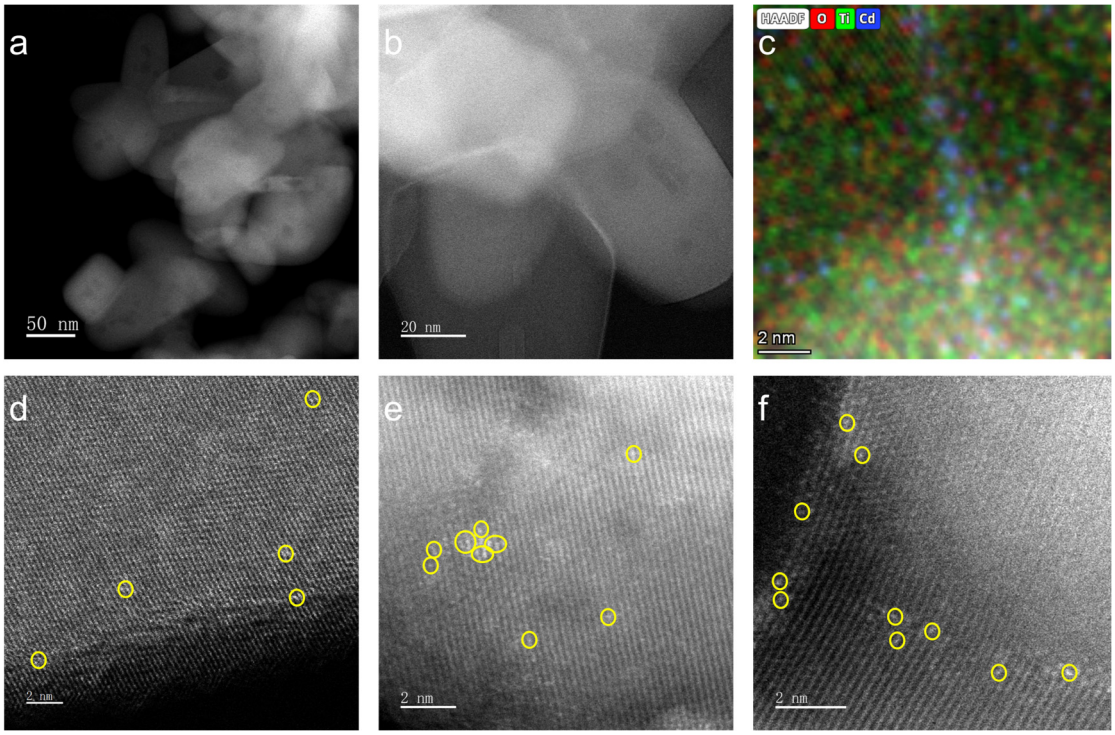

Fig. S11 EDX mapping (**a-c**) and HAADF-STEM (**d-f**) images of the 5Cd/R catalyst. (Cd single atoms were highlighted in yellow).

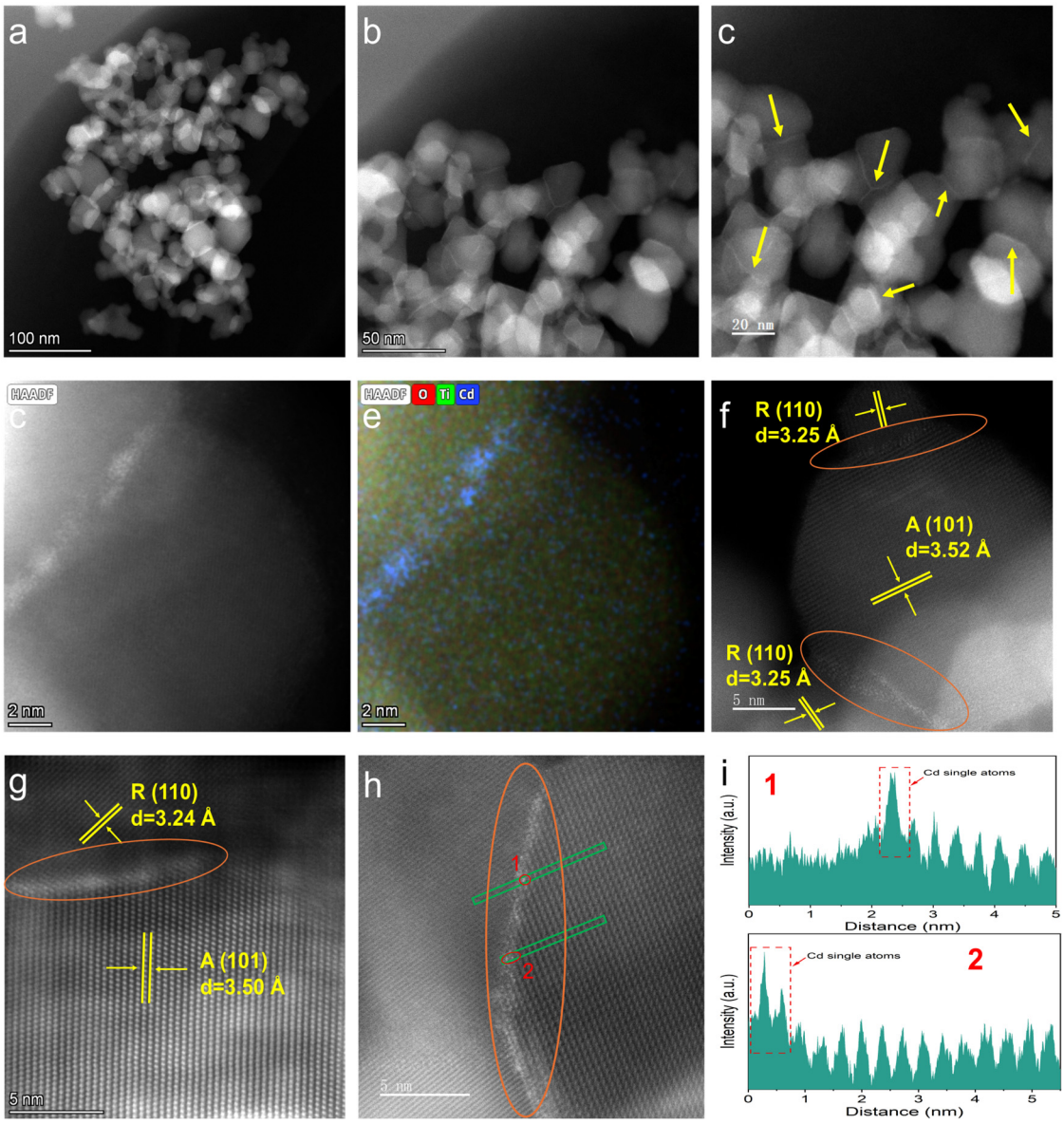

Fig. S12 (**a**-**c**) HAADF-STEM images of the 5Cd/P25 catalyst, scale range 20-100 nm. (**d** and **e**) Corresponding EDX mapping images. (**f**-**h**) HAADF-STEM images of the 5Cd/P25 catalyst at 5 nm, with Cd single atoms anchored between A (101) and R (110) facets (orange markers). (**i**) Intensity profiles along the green lines in (**h**).

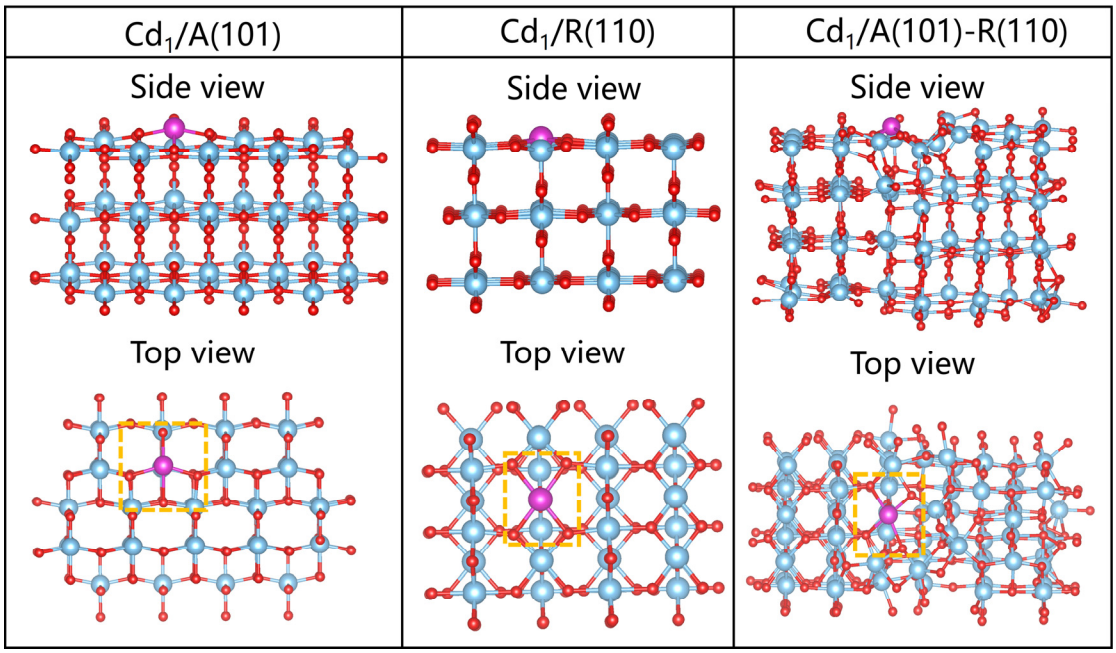

Fig. S13 DFT-derived models of Cd_1/A (101), Cd_1/R (110), and Cd_1/A (101)-R (110) interfaces.

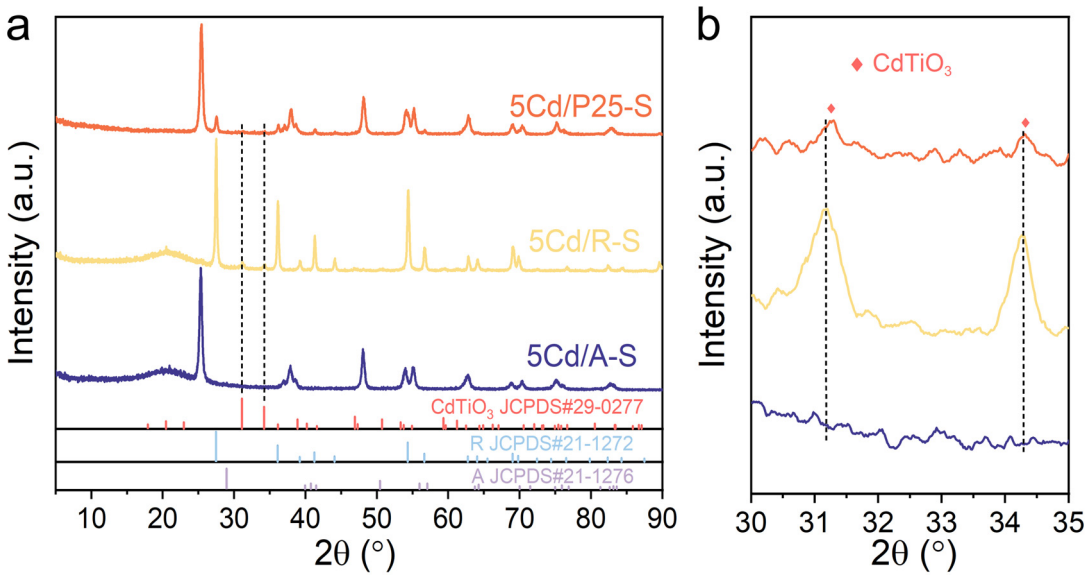

Fig. S14 (**a**) XRD patterns of the spent catalysts. (S represents spent) (**b**) Enlarged view of the XRD patterns within the 2θ range of 30° to 35°.

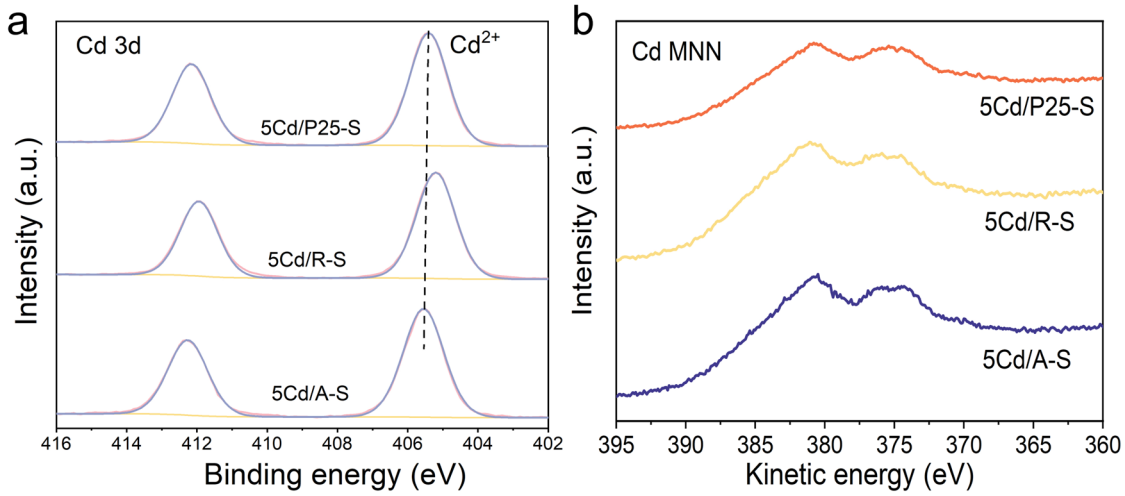

Fig. S15 (**a**) XPS and (**b**) AES spectra of the spent catalysts.

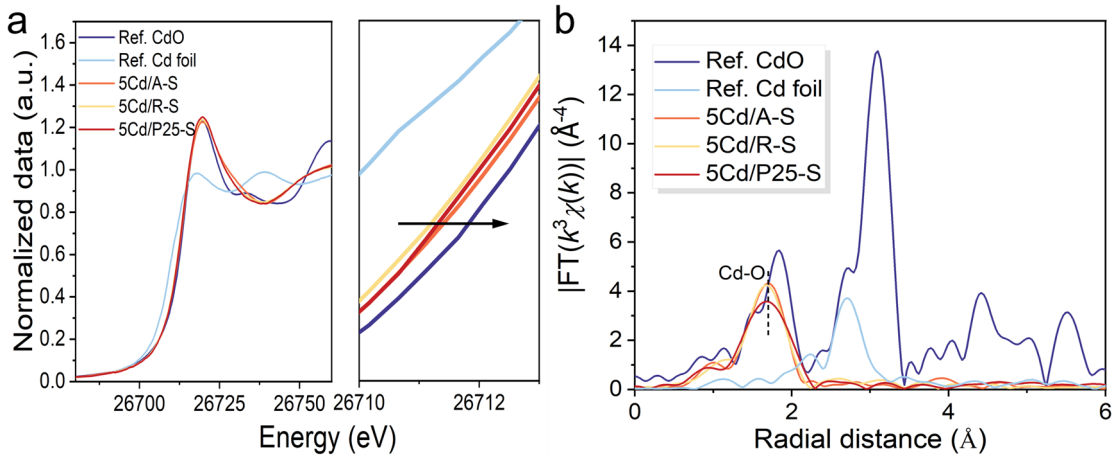

Fig. S16 (**a**) Cd K-edge XANES spectra of the spent catalysts. (**b**) K^3-weighted χ (k) function derived from the EXAFS spectra.

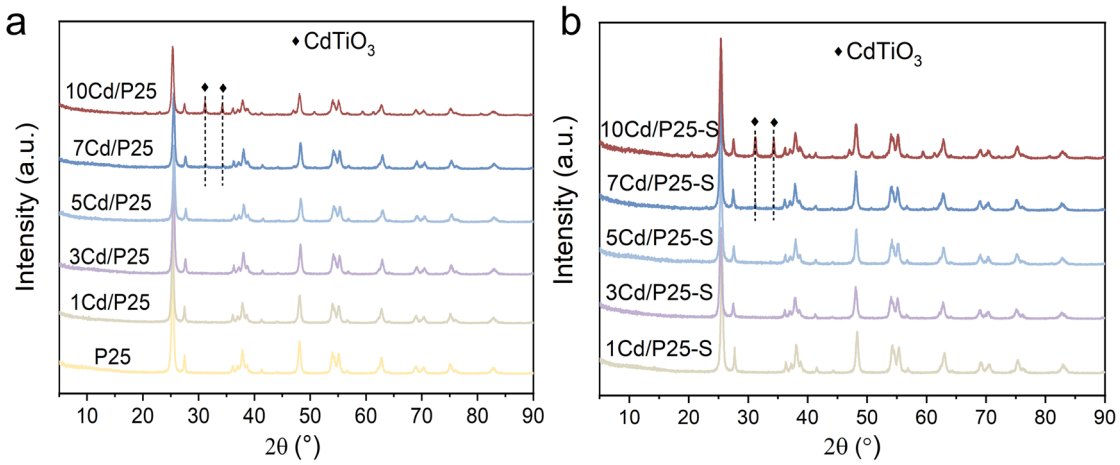

Fig. S17 XRD patterns of catalysts with different Cd loadings. (**a**) Fresh catalysts. (**b**) Spent catalysts.

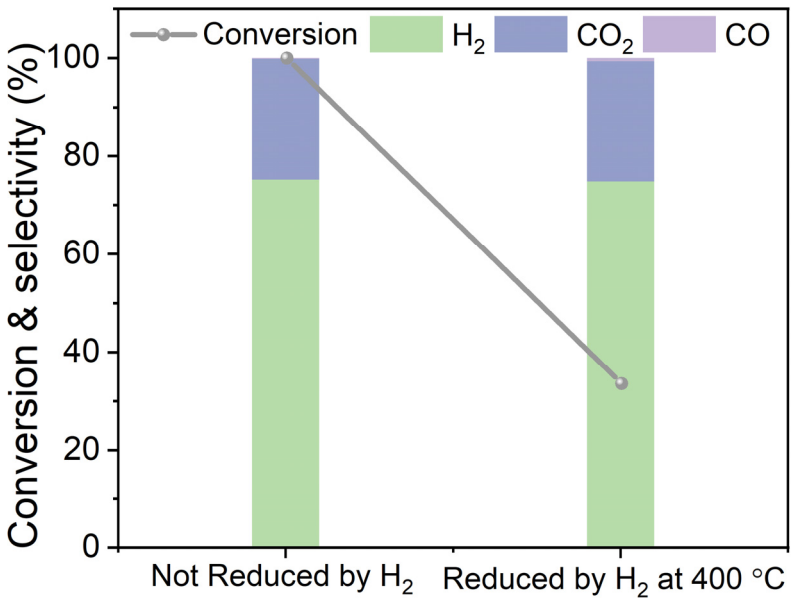

Fig. S18 Influence of H_2 reduction temperature on the catalytic performance of the 5Cd/P25 catalyst. Reduction conditions: 400℃, H_2 (50mL/min), and atmospheric pressure.

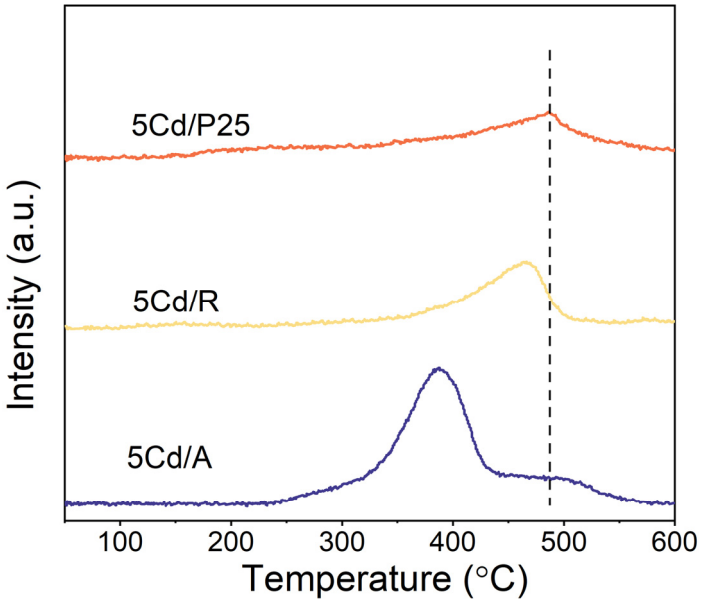

Fig. S19 H_2-TPR profiles of three fresh catalysts.

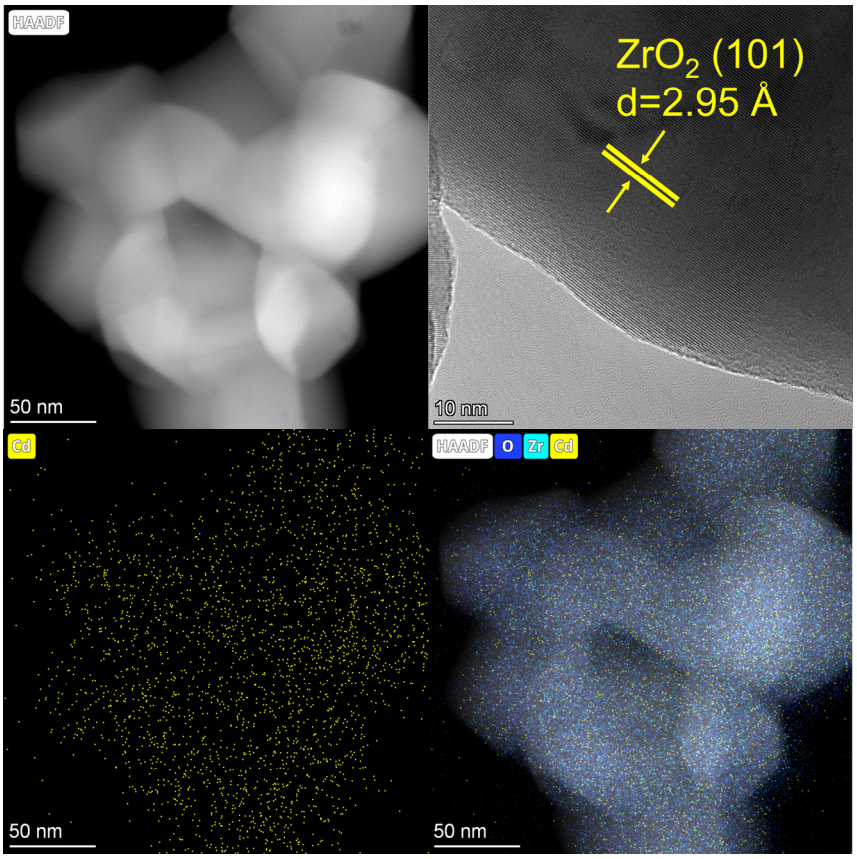

Fig. S20 HAADF, HRTEM, and EDX mapping images of the 5Cd/ZrO_2 catalyst.

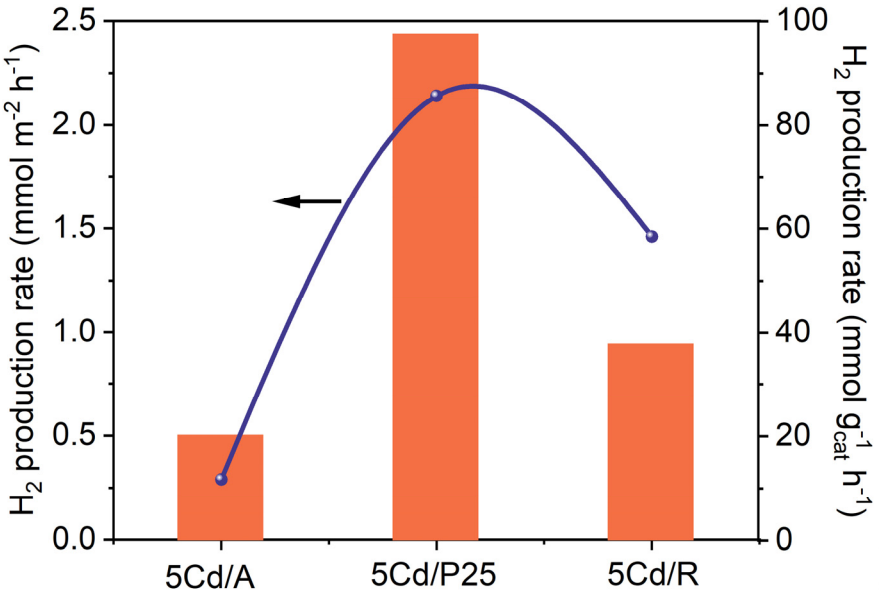

Fig. S21 H_2 production rate normalized to the specific surface area of TiO_2 for a comparative analysis of different catalysts.

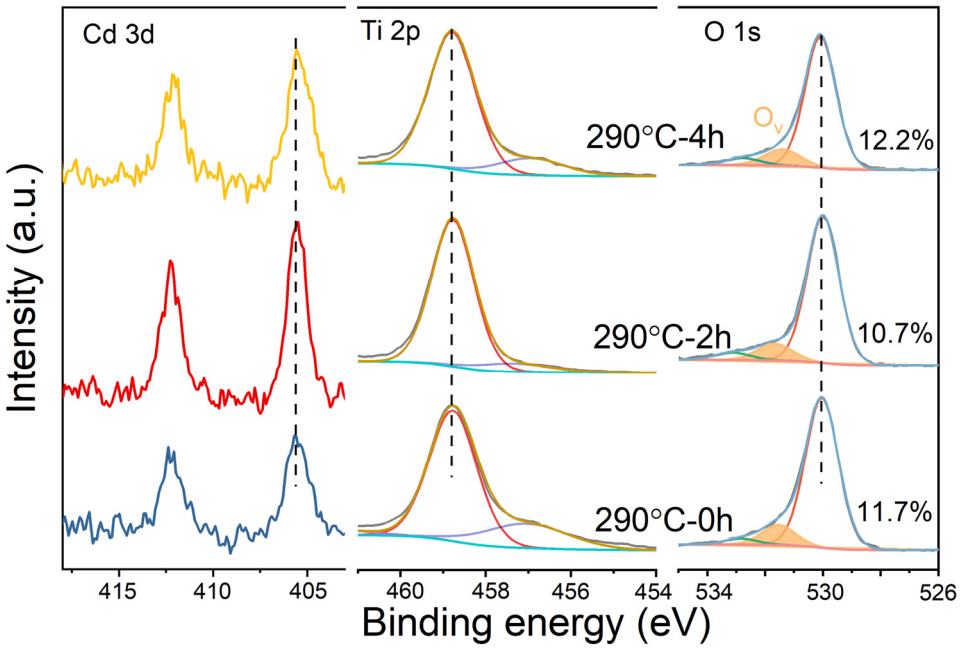

Fig. S22 In situ XPS spectrum of the 5Cd/P25 catalyst during the MSR reaction at 290℃ and a S/C ratio of 3/1.

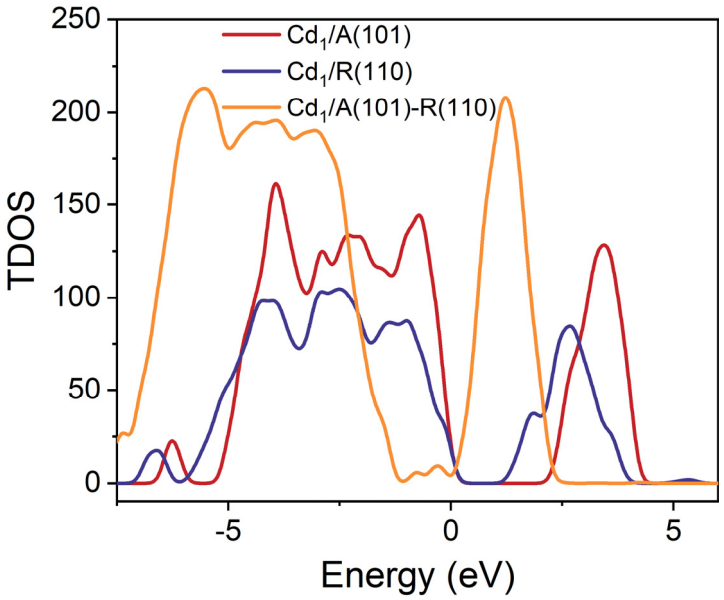

Fig. S23 Total density of states for the Cd_1/A (101), Cd_1/R (110), and Cd_1/A (101)-R (110).

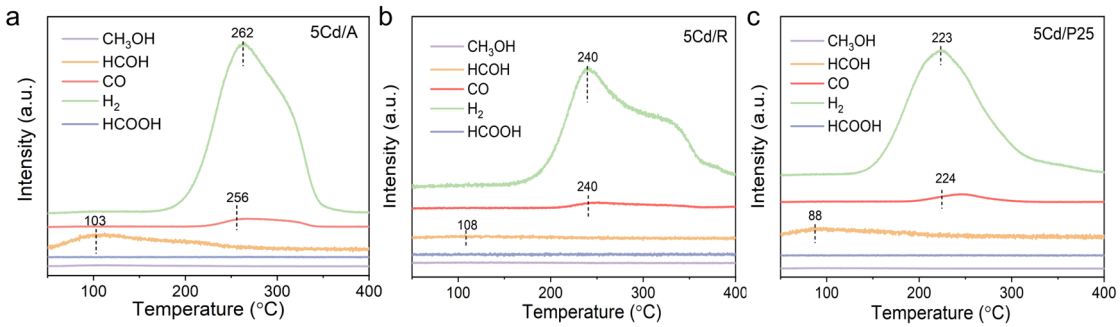

Fig. S24 CH_3OH-TPD profiles of three samples (CH_3OH was decomposed with the increase of temperature).

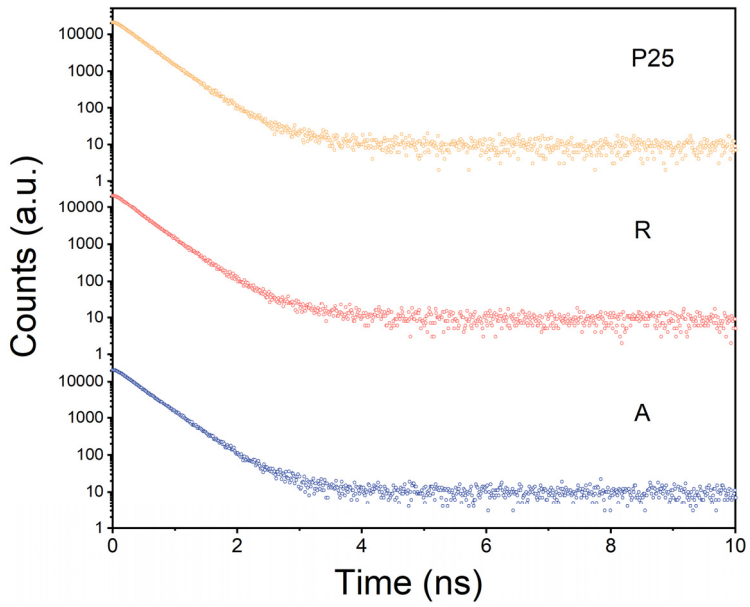

Fig. S25 PALS of A, R, and P25 support materials.

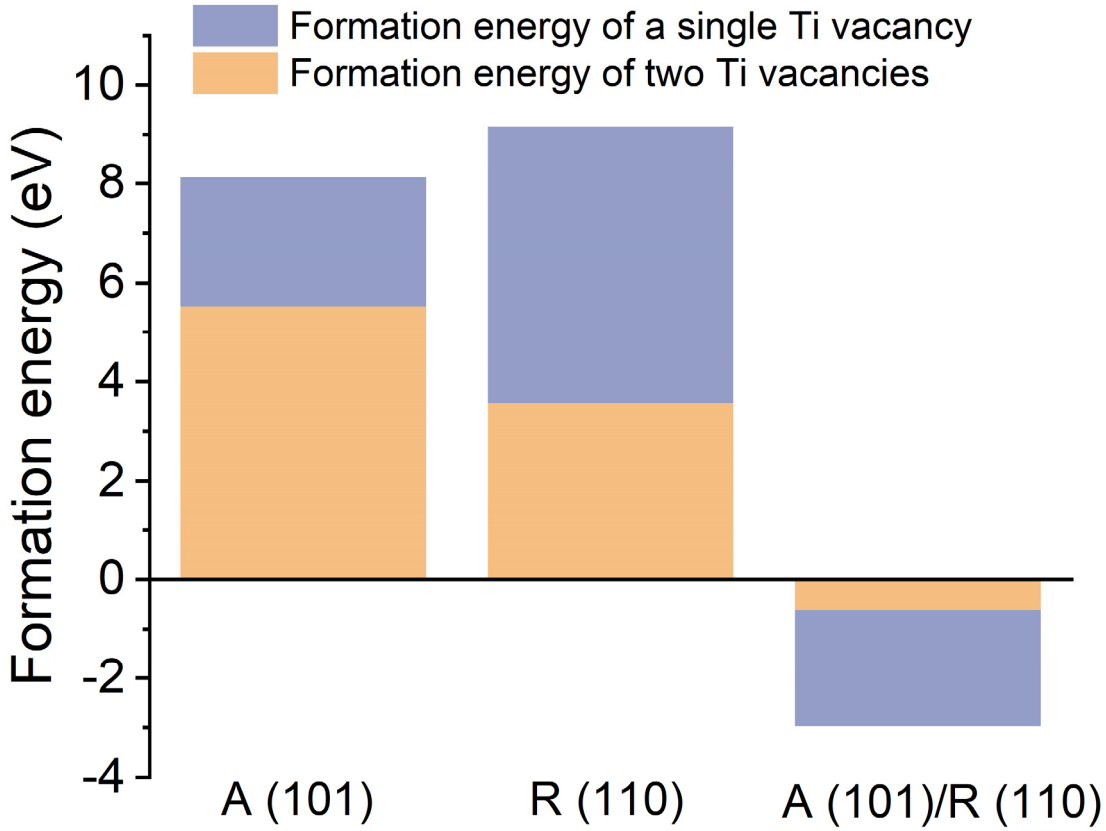

Fig. S26 Ti vacancy formation energies of a single or two Ti vacancies for the A (101), R (110) facets, and the A (101)-R (110) phase junction.

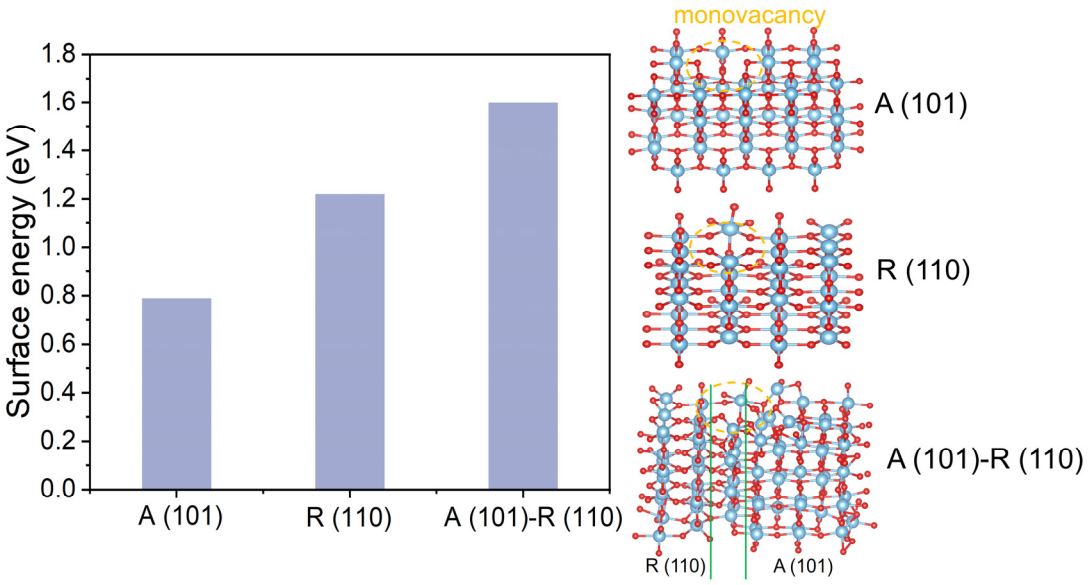

Fig. S27 Surface energy and structure models of the A (101), R (110) facets, and the A (101)-R (110) phase junction with a monovacancy.

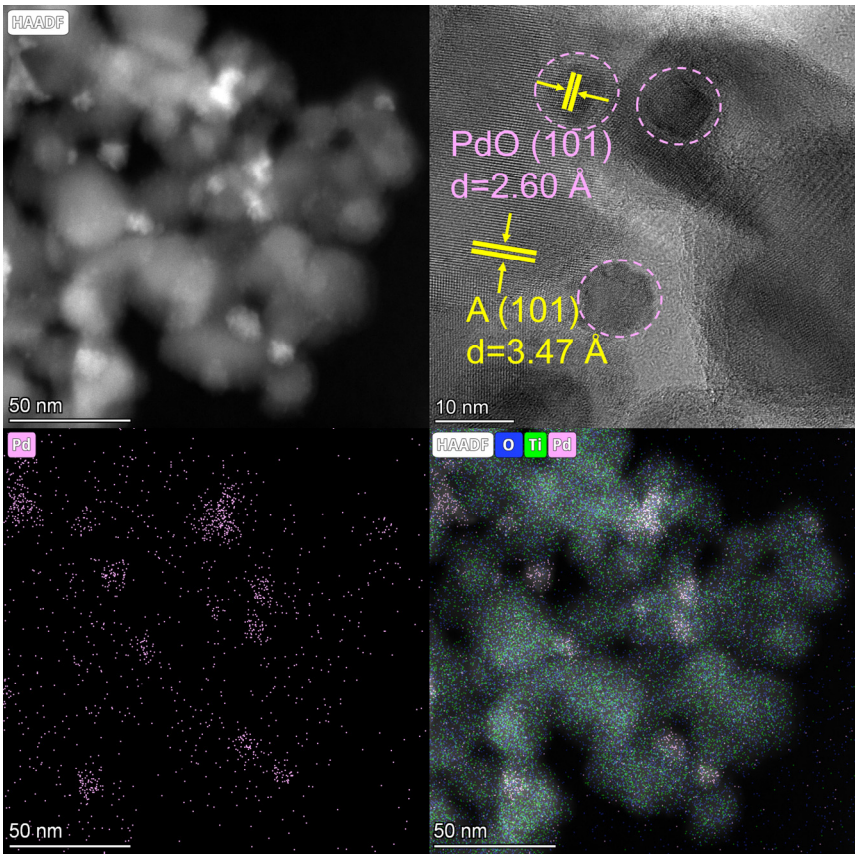

Fig. S28 HAADF, HRTEM, and EDS mapping images of the 5Pd/P25 catalyst.

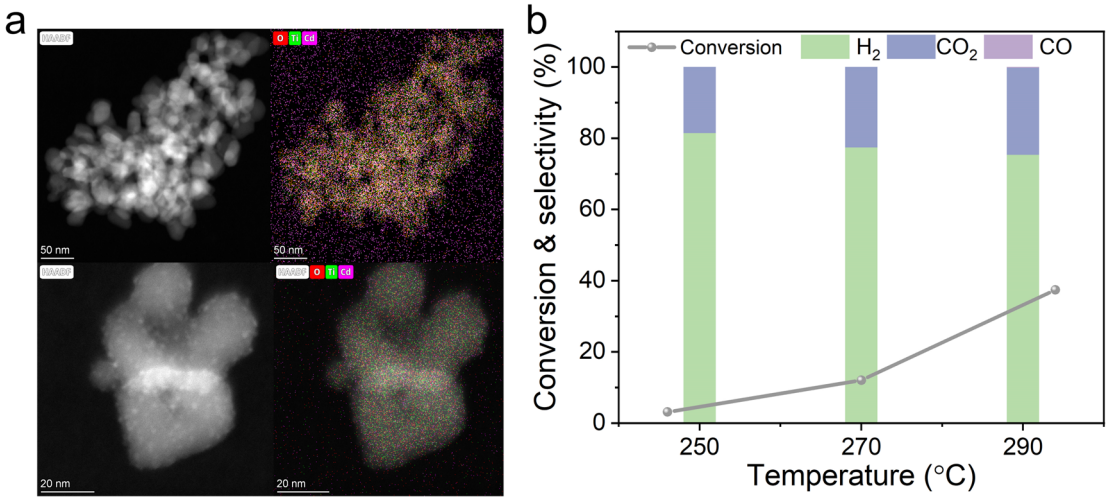

Fig. S29 (**a**) HADDF and EDS mapping images of the 5Cd/80A-20R catalyst. (**b**) Corresponding methanol conversion and product selectivity under the following reaction conditions: temperatures ranging from 250 to 290°C, an S/C ratio of 3/1, 0.1 MPa pressure, and a feed rate of 3 mL g^{-1} h^{-1}.

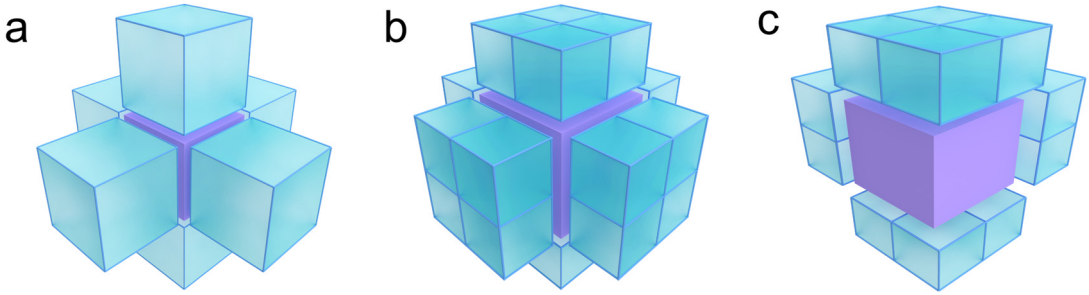

Fig. S30 Schematic representations of three size models with anatase (A) stacked on rutile (R). (**a**) The two cubes are equal in size. (**b**) R is twice the size of A. (**c**) A is twice the size of R (blue cubes: A; purple cubes: R).

Based on TEM images revealing the irregular shape of catalyst particles, we approximated the catalysts as stacked cubes of anatase (A) and rutile (R). The particle size and phase ratio, which can be tuned via N_2 and H_2 pretreatments, influence the interface density between particles. Therefore, the theoretical interface density can be deduced from the contact area of these stacked cubes. The particle size and phase ratio were determined using the Scherrer equation, as detailed in Table S7. Given the larger particle size of R relative to A, the model further reduces to the scenario where A is stacked on R, with the maximum contact area constrained by the dimensions of R. If A and R are of equal size, the maximum contact number is 6 (Fig. S27A); If R is twice the size of A, this number doubles to 24 (Fig. S27B). Therefore, the maximum contact number (CN_{max}) can be calculated as follows:

$$CN_{max} = \frac{S(R)}{S(A)} \times 6 = \frac{a^2(R)}{a^2(A)} \times 6$$

Where a is the cube size (crystal size); Since the size of the R does not exceed twice that of the A, the CN_{max} ranges from 6 to 24 (Fig. S27C).

The N is defined as the particle number of A or R, which was determined by the phase ratio.

$$N(A) = \frac{w_A}{\rho_A a(A)^3} \qquad N(R) = \frac{w_R}{\rho_R a(R)^3}$$

Where w is the weight fraction, ρ is the respective crystal density (ρ_R: 4.2 g/cm^3; ρ_R: 4.2 g/cm^3), and a refers to the cube size (crystal size). The data is presented in Table S8.

Our model does not consider the specific dispersion of particles observed in practical scenarios, such as clusters of adjacent R particles. Therefore, as illustrated in Fig. S27, the theoretical maximum interface density (A_{max}) is derived from the subsequent equation under conditions where the ratio N(A)/N(R) is greater than CN_{max} (where the quantity of A significantly outnumbers rutile R, yet not every A cube contacts with R).

$$A_{max} = 6 \times N(R) \times a(R)^2$$

Catalysts pretreated with N_2 at 500 °C for 2 hours align with the aforementioned equation.

When the ratio of N(A)/N(R) is less than CN_{max}, full contact between A and R is possible. The A_{max} can then be calculated using the following formula:

$$A_{max} = \frac{N\ (A)/N\ (R)}{CN_{max}} \times 6 \times N(R) \times a(R)^2$$

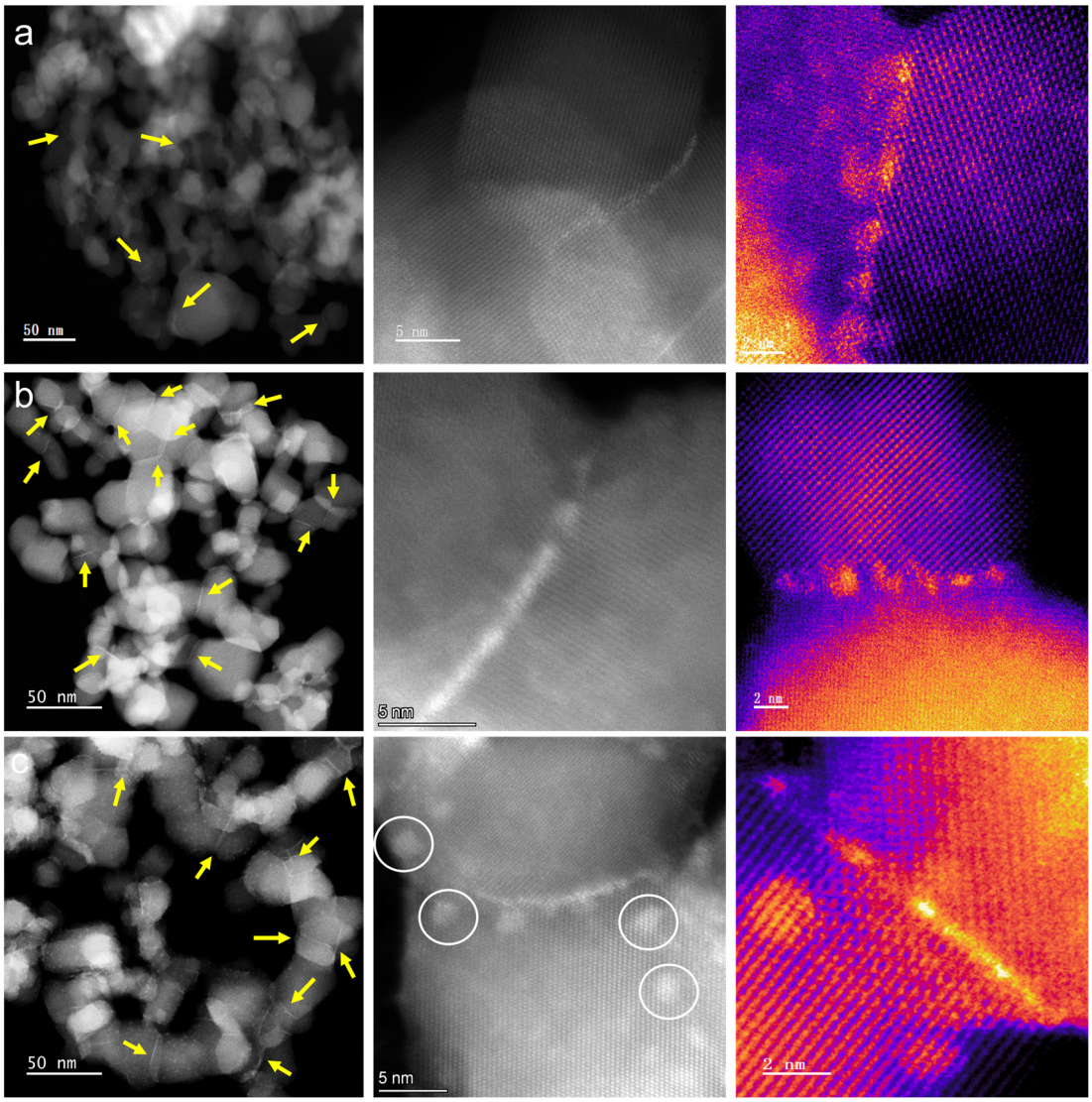

Fig. S31 HADDF-STEM images of the 5Cd/P25 catalyst following H_2 pretreatment for (**a**) 0 h, (**b**) 4 h, and (**c**) 8 h.

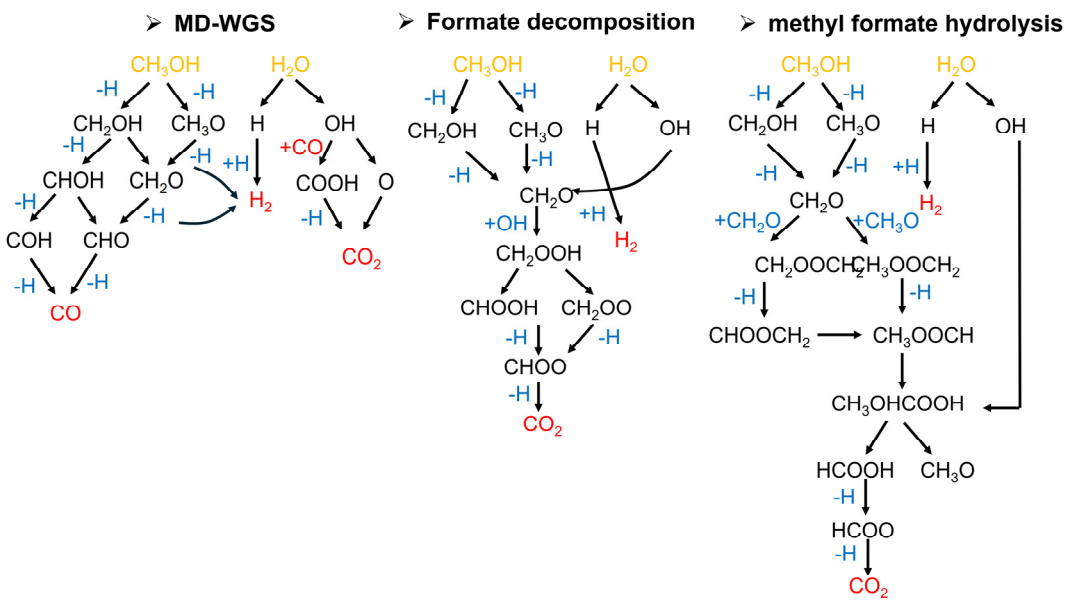

Fig. S32 Schematic representation of the three MSR reaction pathways.

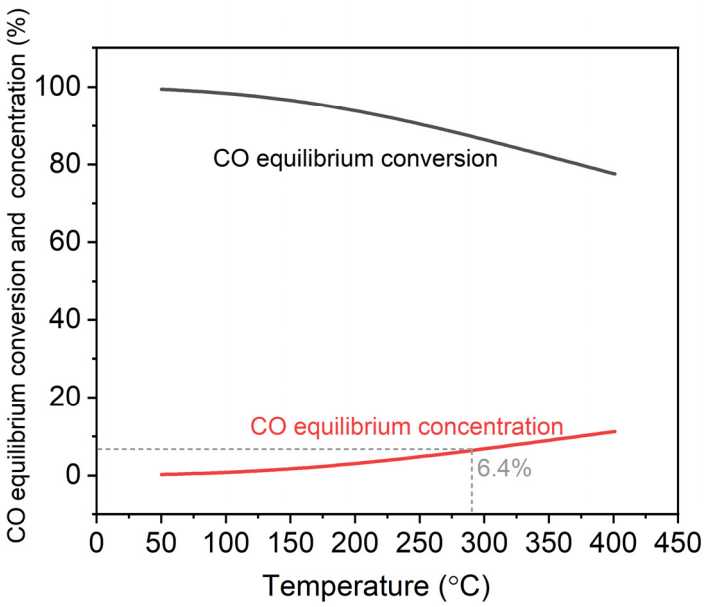

Fig. S33 Equilibrium conversion and concentration profiles for CO in the water-gas shift (WGS) reaction.

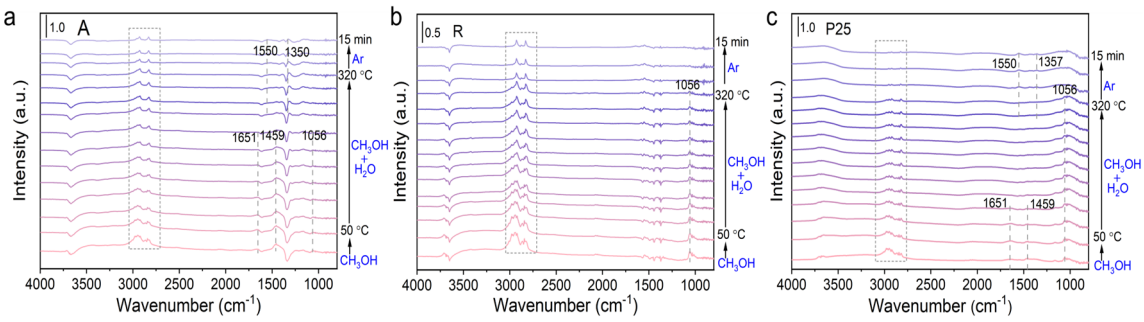

Fig. S34 In situ DRIFTS of A, R, and P25 supports during the MSR reaction.

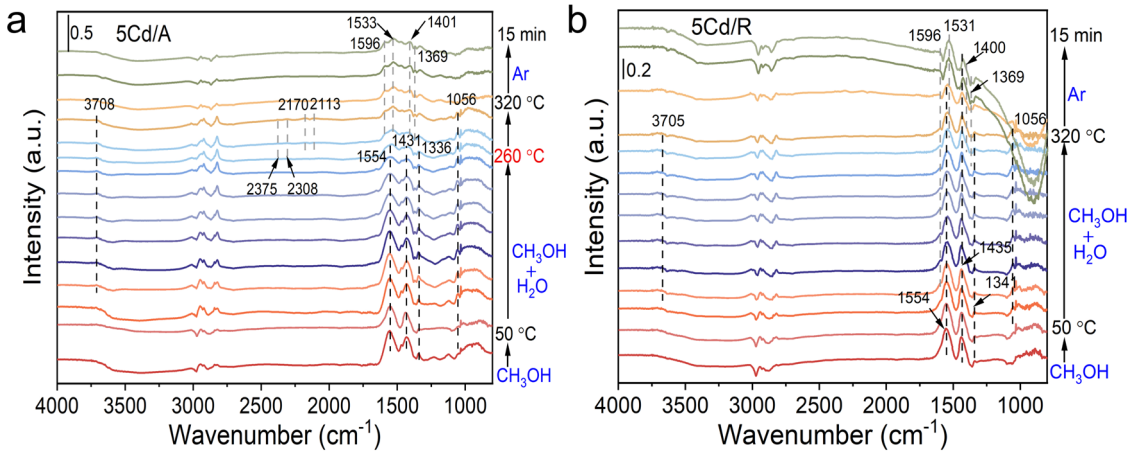

Fig. S35 In situ DRIFTS of the 5Cd/A and 5Cd/R catalysts during the MSR reaction.

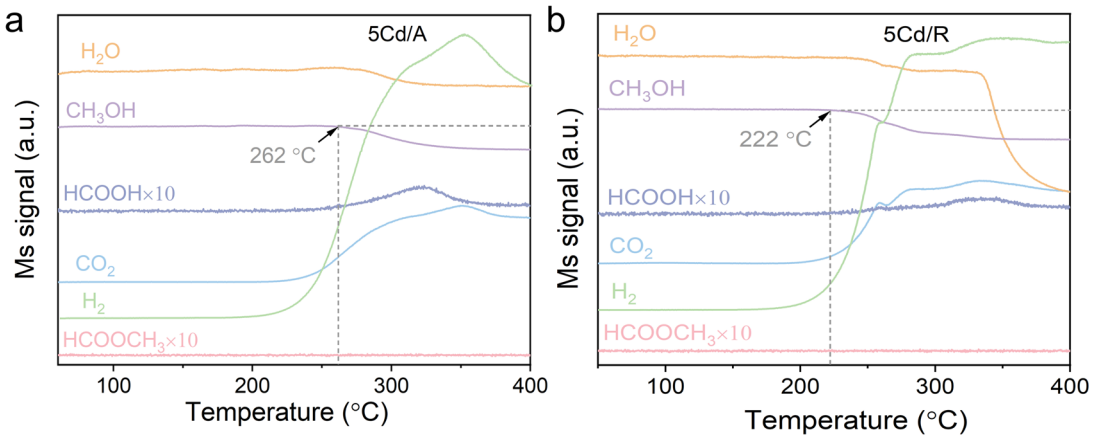

Fig. S36 TPSR profiles of the 5Cd/A (**a**) and 5Cd/R (**b**) catalysts.

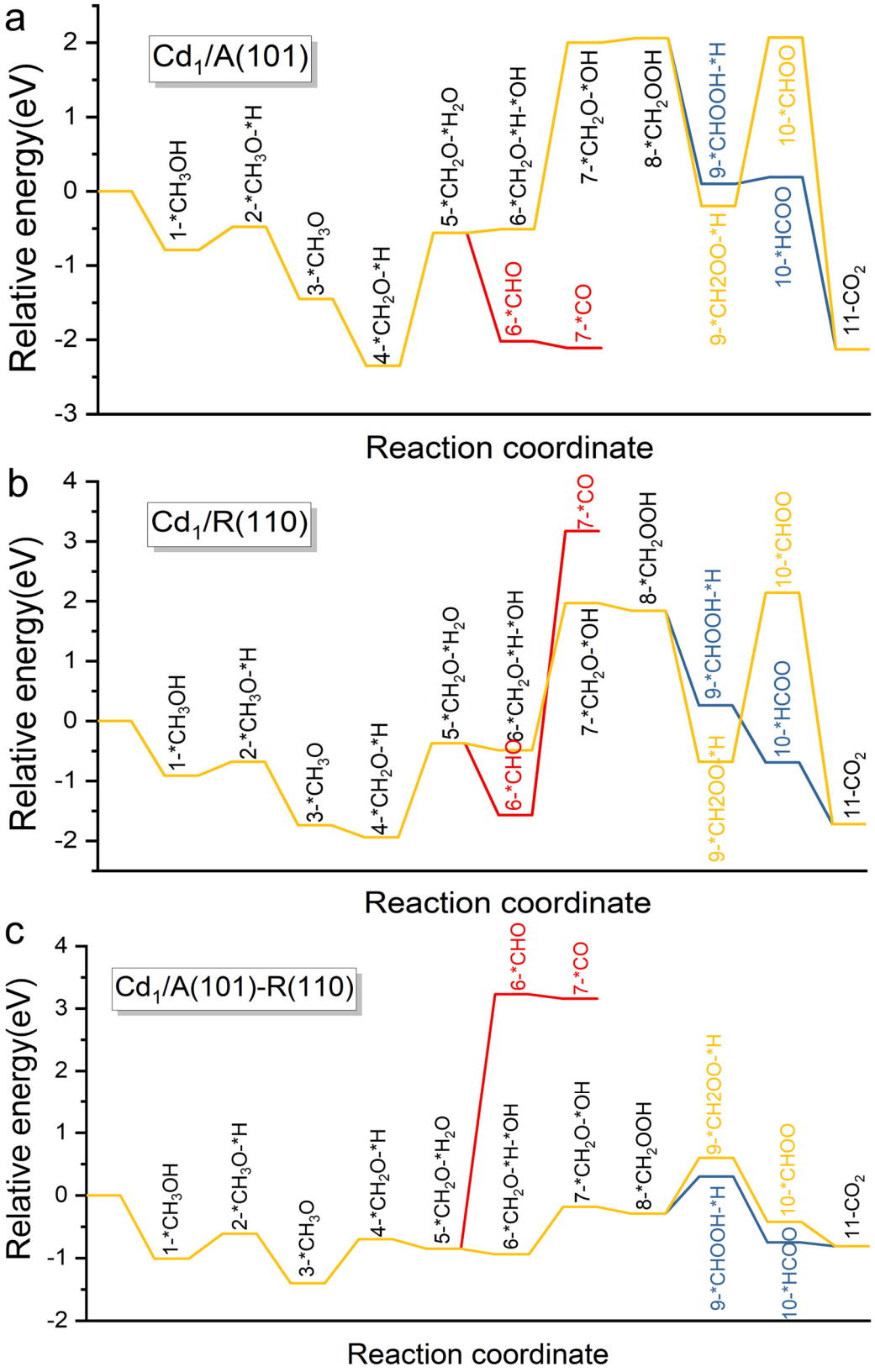

Fig. S37 Energy landscapes for the single-atom catalyst configurations: (**a**) Cd_1/A (101), (**b**) Cd_1/R (110), and (**c**) Cd_1/A (101)-R (110).

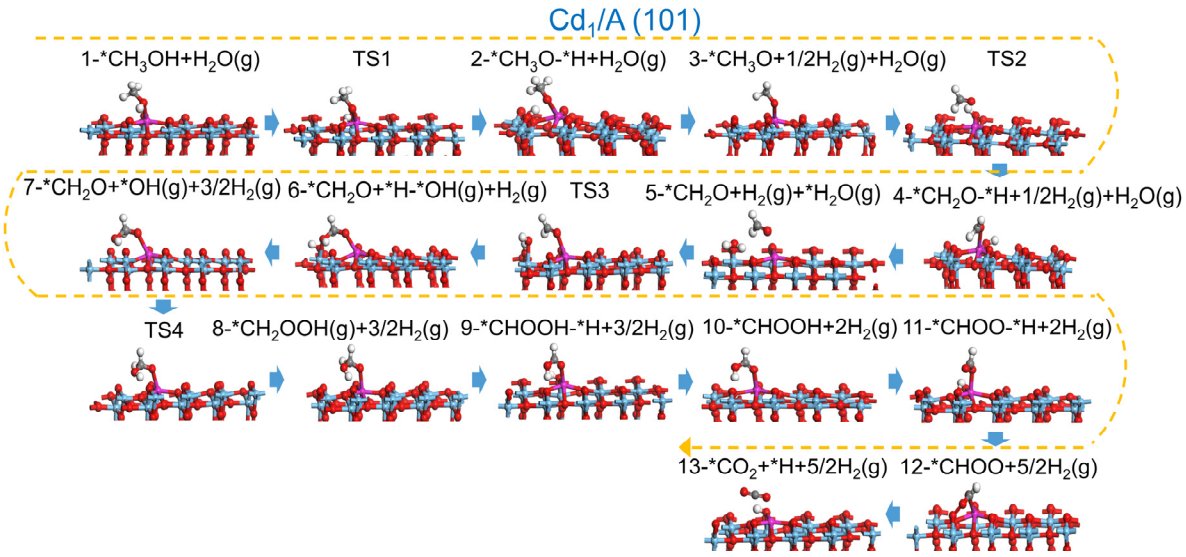

Fig. 38 Atomic models illustrating the formate decomposition pathway on Cd_1/A (101) during the MSR reaction.

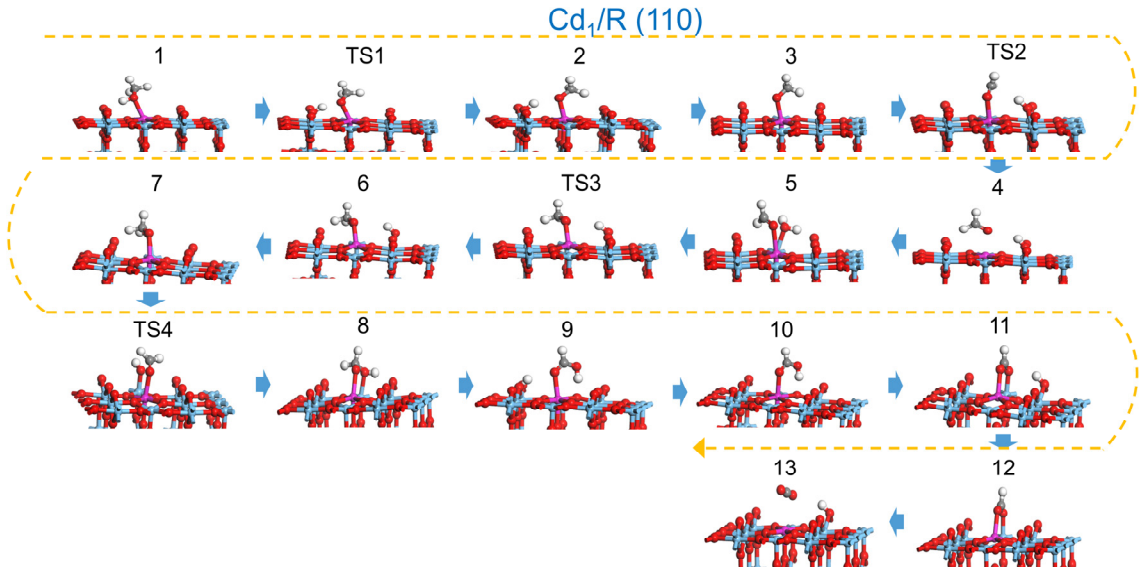

Fig. 39 Atomic models illustrating the formate decomposition pathway on Cd_1/R (110) during the MSR reaction.

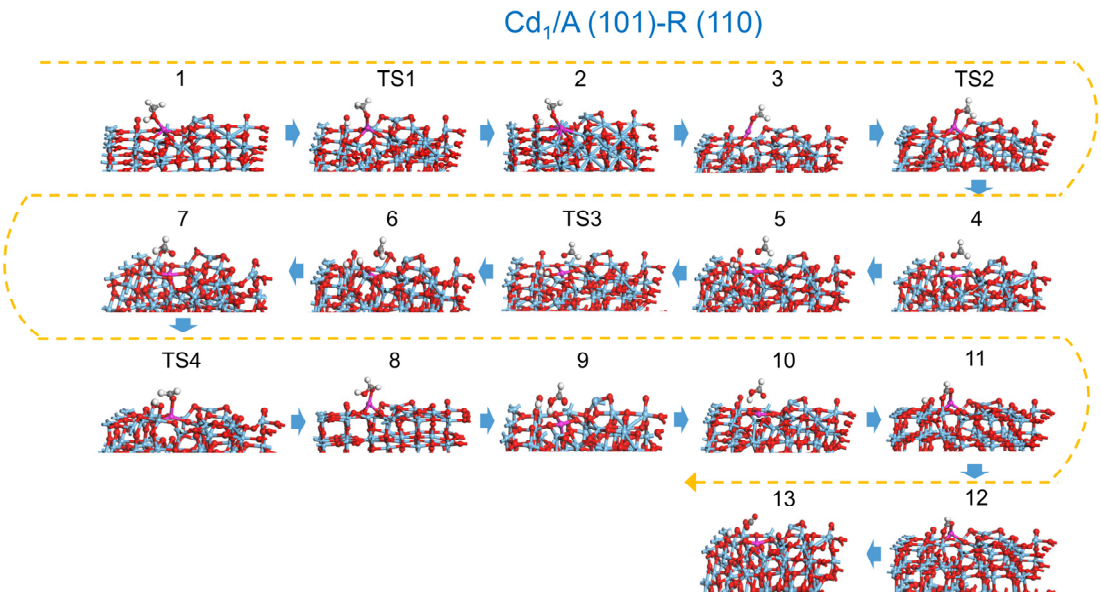

Fig. 40 Atomic models illustrating the formate decomposition pathway on Cd_1/A (101)-R (110) during the MSR reaction.

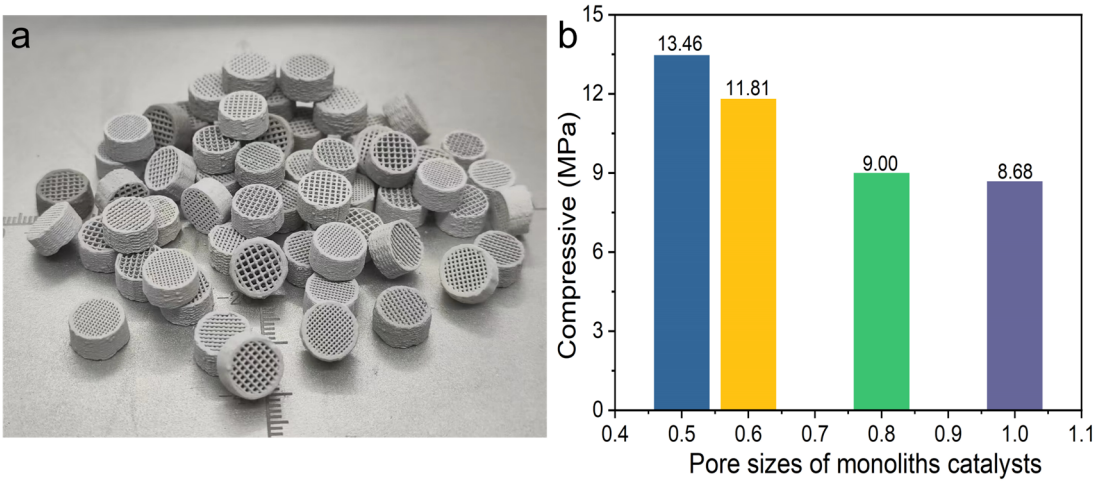

Fig. S41 (**a**) 3D printed kilogram-scale 5Cd/P25 catalysts. (**b**) Compressive strength of 3D-printed monolithic catalysts with varying pore sizes.

Fig. S42 Custom-sizing of 3D-printed catalysts to fit specific reactor dimensions.

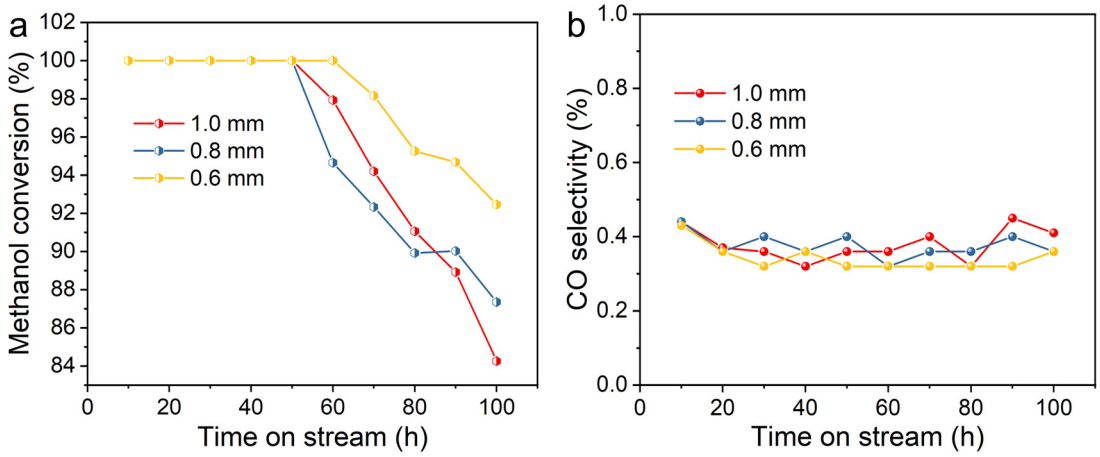

Fig. S43 Methanol conversion (**a**) and CO selectivity (**b**) of 3D-printed 5Cd/P25 catalysts with different pore sizes.

Note: The larger pore size in 3D printing affected its stability, which is likely due to structural collapse.

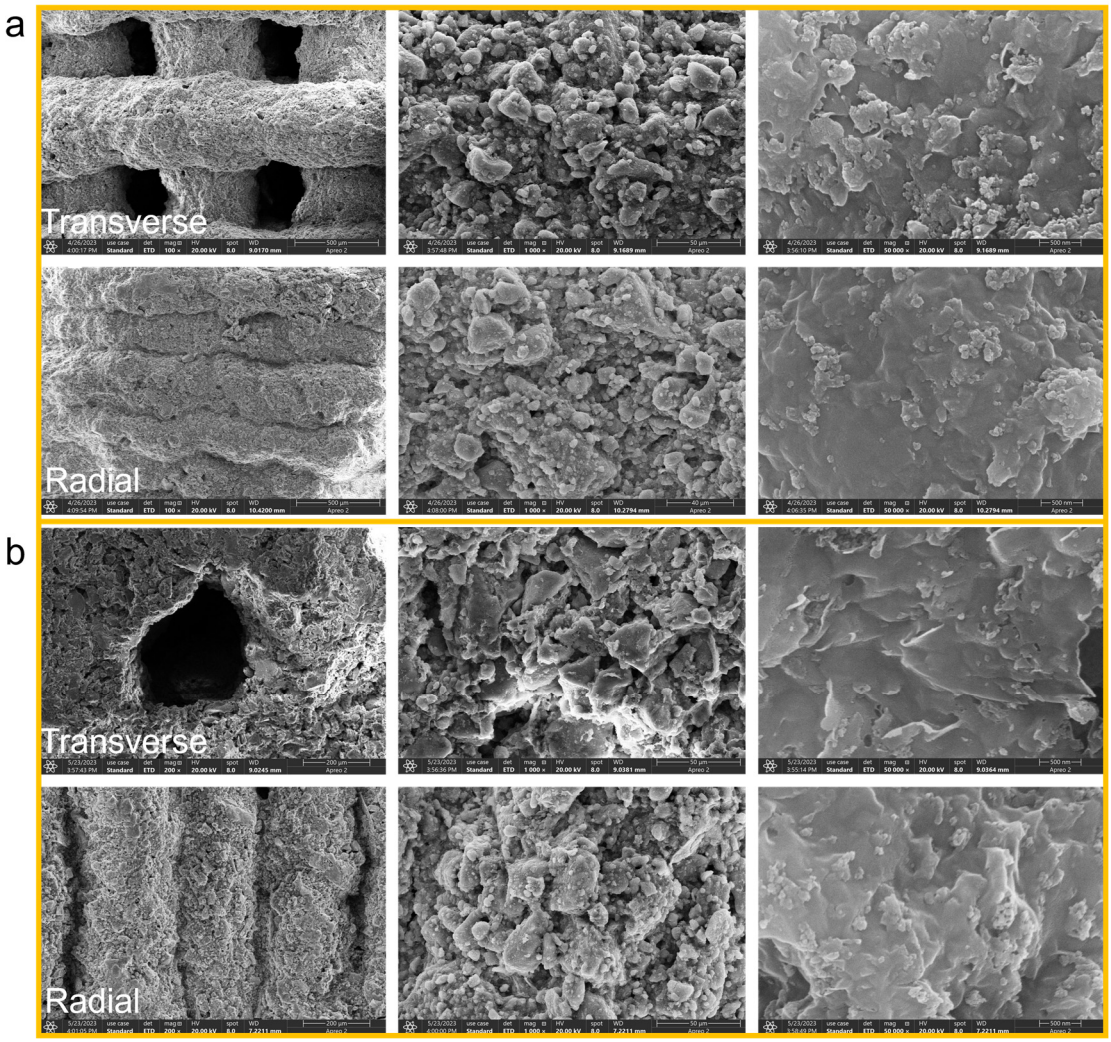

Fig. S44 SEM images of the 3D-printed 5Cd/P25 catalysts with a pore size of 0.5 mm, showing (**a**) fresh and (**b**) spent catalysts.

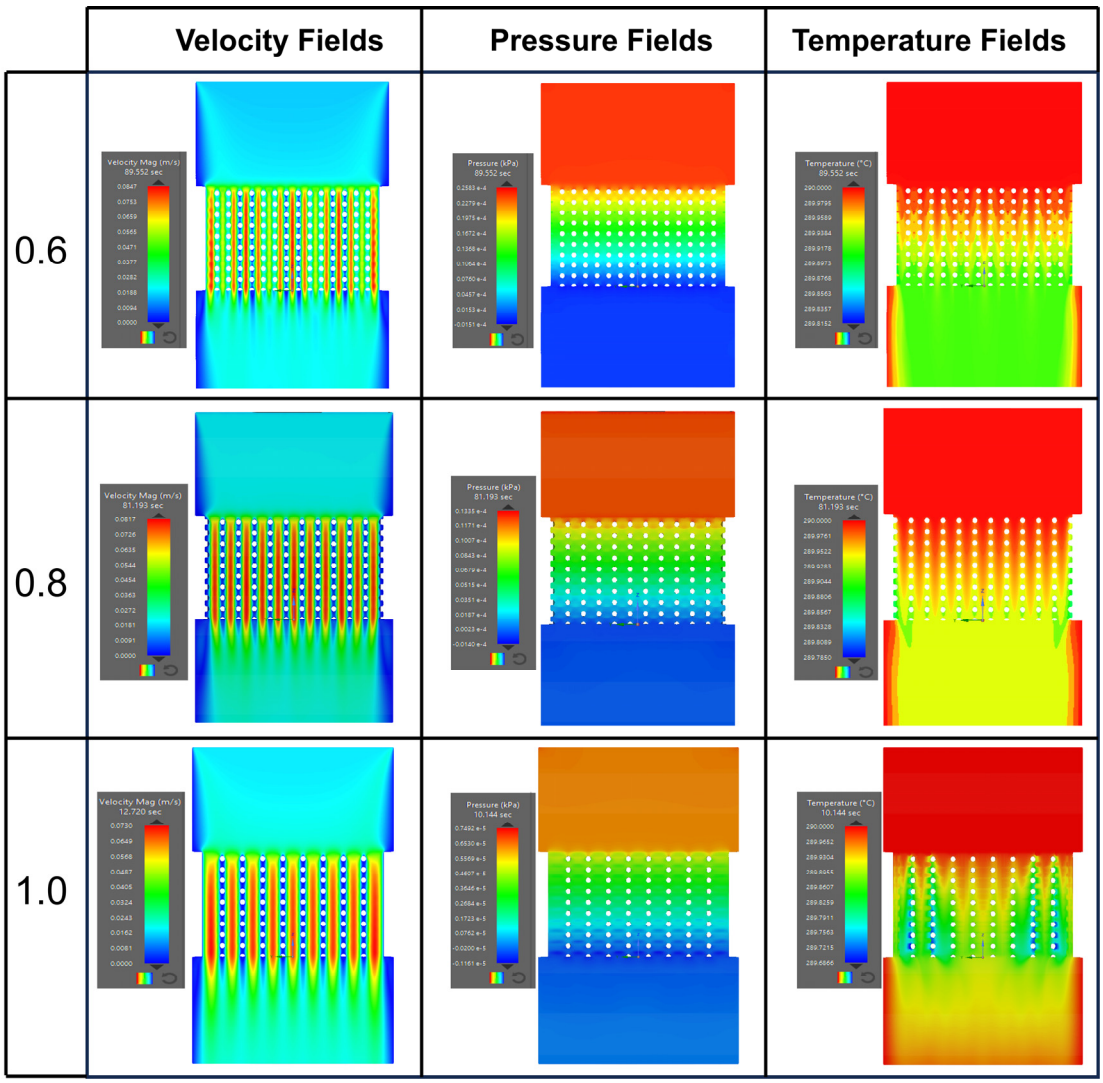

Fig. S45 CFD simulation of mass and heat transfer in monolithic catalysts. Simulated velocity, pressure, and temperature fields for 3D-printed Cd/TiO_2 catalysts with pore sizes of 0.6 mm, 0.8 mm, and 1.0 mm, respectively.

Table S1 Lattice mismatch between cadmium oxides and anatase/rutile.

	Lattice constant (a)	Lattice mismatch ($\Delta\delta$)*
Anatase	3.7842	24.1%
Rutile	4.5845	2.4%
CdO	4.69599	-

*The lattice mismatch was calculated by the formulate:

$$\Delta\delta = \frac{a_{Cd} - a_{TiO_2}}{a_{TiO_2}}$$

Table S2 EXAFS fitting parameters at the Cd *K*-edge for various samples (S_0^2=0.769).

Samples	Shell	CN^a	R(Å)^b	σ^2(Å^2)^c	ΔE_0(eV)^d	*R* factor
Cd foil	Cd-Cd	6*	2.939±0.006	0.0124±0.0008	3.0±0.8	0.0081
CdO	Cd-O	6.0±0.4	2.322±0.016	0.0082±0.0013	1.9±2.2	0.0184
	Cd-Cd	12.0±0.5	3.322±0.004	0.0080±0.0005		
5Cd/A	Cd-O	6.2±0.2	2.245±0.004	0.0099±0.0007	1.4±0.3	0.0016
5Cd/R	Cd-O	5.4±0.5	2.237±0.012	0.0090±0.0020	0.9±0.9	0.0108
5Cd/P25	Cd-O	5.8±0.5	2.236±0.010	0.0098±0.0018	0.6±0.8	0.0057

[a]*CN*: Coordination number; [b]*R*: Distance to the neighboring atom; [c]σ^2: Mean square relative displacement (MSRD); [d]ΔE_0: Inner potential correction; *R* factor indicates the goodness of the fit. S_0^2 was fixed to 0.769, according to the experimental EXAFS fit of Cd foil by fixing *CN* as the known crystallographic value. * This value was fixed during EXAFS fitting, based on the known structure of Cd.

Fitting range:

For Cd foil: $3.0 \le k$ (/Å) ≤ 12.3 and $1.0 \le R$ (Å) ≤ 3.5;

For 5Cd/A: $2.0 \le k$ (/Å) ≤ 11.3 and $1.0 \le R$ (Å) ≤ 2.5;

For 5Cd/R: $2.0 \le k$ (/Å) ≤ 10.6 and $1.0 \le R$ (Å) ≤ 2.5;

For 5Cd/P25: $2.0 \le k$ (/Å) ≤ 10.0 and $1.0 \le R$ (Å) ≤ 2.5.

A reasonable range of EXAFS fitting parameters: $0.700 < S_0^2 < 1.000$; $CN > 0$; $\sigma^2 > 0$ Å^2; $|\Delta E_0| <$ 10 eV; *R* factor < 0.02.

Table S3 EXAFS fitting parameters at the Cd *K*-edge for the spent catalysts (S_0^2=0.775).

Samples	Shell	CN[a]	R(Å)[b]	σ^2(Å^2)[c]	ΔE_0(eV)[d]	R factor
Cd foil	Cd-Cd	6*	2.940±0.011	0.0115±0.0009	-0.5±2.7	0.0067
CdO	Cd-O	6.0±0.4	2.322±0.016	0.0082±0.0013	1.9±2.2	0.0184
	Cd-Cd	12.0±0.5	3.322±0.004	0.0080±0.0005		
5Cd/A-S	Cd-O	6.3±0.7	2.250±0.011	0.0095±0.0017	1.0±1.1	0.0041
5Cd/R-S	Cd-O	6.2±0.6	2.251±0.009	0.0103±0.0014	1.4±1.0	0.0083
5Cd/P25-S	Cd-O	5.9±0.2	2.256±0.021	0.0111±0.0037	1.5±1.9	0.0074

[a]*CN*: Coordination number; [b]*R*: Distance to the neighboring atom; [c]σ^2: Mean square relative displacement (MSRD); [d]ΔE_0: Inner potential correction; *R* factor indicates the goodness of the fit. S_0^2 was fixed to 0.775, according to the experimental EXAFS fit of Cd foil by fixing *CN* as the known crystallographic value. * This value was fixed during EXAFS fitting, based on the known structure of Cd.

Fitting range:

For Cd foil: $3.0 \le k$ (/Å) ≤ 13.6 and $1.8 \le R$ (Å) ≤ 3.5;

For 5Cd/A-S: $2.0 \le k$ (/Å) ≤ 11.5 and $1.2 \le R$ (Å) ≤ 2.5;

For 5Cd/R-S: $1.0 \le k$ (/Å) ≤ 11.0 and $1.1 \le R$ (Å) ≤ 2.5;

For 5Cd/P25-S: $2.5 \le k$ (/Å) ≤ 9.6 and $1.2 \le R$ (Å) ≤ 2.5.

A reasonable range of EXAFS fitting parameters: $0.700 < S_0^2 < 1.000$; $CN > 0$; $\sigma^2 > 0$ Å^2; $|\Delta E_0| <$ 10 eV; *R* factor < 0.02.

Table S4 Catalytic performance of homemade reference catalysts.

Catalyst	**Conversion (%)**	**S_{CO2}**	**S_{CO}**	**S_{CH4}**
$CdTiO_3$	0	0	0	0
CdO	0.1	0	100	0
Cd	0	0	0	0

Reaction conditions: 290°C, 0.1 MPa, a S/C ratio of 3/1, and a feed rate of 3 mL g^{-1} h^{-1}

Table S5 Texture properties of fresh catalysts.

Catalysts	**BET surface area (m^2/g)**	**Pore volume (cm^3/g)**	**Average pore diameter (nm)**
A	85.54	0.35	16.51
R	36.10	0.19	21.22
P25	51.82	0.31	23.29
5Cd/A	70.91	0.24	13.21
5Cd/R	26.00	0.09	14.29
5Cd/P25	45.60	0.36	31.65

Table S6 Positron lifetimes and relative intensities of samples.

Catalyst	τ_1(ps)	I_1(%)	τ_2(ps)	I_2(%)
A	245	16.0	374	84.0
R	217	26.4	386	73.6
P25	212	7.3	364	92.7

Table S7 Ionic radius and electronegativities of the metals.

Metals	**Ionic radius (Å)**	**Electronegativity**
Cd	0.97 (2+, six coordination)	1.69
Pd	0.86 (2+, six coordination)	2.20
Pt	0.62 (4+, six coordination)	2.28
Cu	0.73 (2+, six coordination)	1.90
Ti	0.61 (4+, six coordination)	1.54

Table S8 Data for interface density calculations following the N_2 and H_2 pretreatments of P25.

Pretreatment	**Temperature /Time**	**W_A /%**	**W_R /%**	**crystal size /nm**		**CN_{max}**	**N (A) /10^{15} g^{-1}**	**N (R) /10^{15} g^{-1}**	**N (A) / N (R)**	**A_{max} /m^2 g^{-1}**
				A	R					
N_2	500℃/2h	79.6	20.4	19.2	36.7	21.9	29.6	0.9	30.1	7.9
	600℃/2h	69.9	30.1	21.7	36.9	17.3	18.0	1.4	12.6	8.5
	700℃/2h	29.6	70.4	33.0	48.4	12.9	2.2	1.5	1.5	2.4
H_2	500℃/2h	73.6	26.4	19.6	21.6	7.3	25.7	6.2	4.1	9.9
	500℃/4h	68.4	31.6	17.9	24.8	11.5	31.4	4.9	6.4	10.1
	500℃/8h	51.3	48.7	21.5	22.5	6.6	13.6	10.2	1.3	6.3

Table S9 Comparison of the MSR performance of the 5Cd/P25 and other reported catalysts.

Catalysts	**Temperature (°C)**	**S/C**	**Pressure (MPa)**	**C_{MeOH} (%)**	**S_{CO} (%)**	**H_2 production rate (mmol g_{cat}^{-1} h^{-1})**	**Tolerance**	**References**
Commercial $Cu/ZnO/Al_2O_3$	300	3.1	0.1	55.0	2.0	100.2	deactivation	[1]
CuZnAl-R10	225	1.3	0.1	67.0	-	-	10% loss after 40h	[2]
Cu/ZnO	240	1.3	0.1	78.8	0.2	238.0	Stable at least 50h	[3]
Cu-Mn spinel oxides	260	1.3	0.1	92.9	0.7	284.0	5% loss after 40h	[4]
Cu/CeO_2	260	1.0	0.1	90.7	2.3[a]	242.4	deactivation	[5]
$Cu/ZnO/ZrO_2/Al_2O_3$	260	0.3	0.1	90.0	0.1	-	10% loss after 5h	[6]
Cu-CoO	240	1.0	0.1	-	9-17	1.0	-	[7]
2Pt/α-MoC	190	2.0	2.0	-	0.06	466.6	deactivation	[8]
0.5Zn-Pt/MoC	160	3.0	0.1	65.9	-	106.9	deactivation	[9]
Ni2.4/Mo97.6C	300	1.0	0.1	100.0	~5.0	81.0	10% loss after 50h	[10]
Pt/TS-1	250	3.0	0.1	-	-	~15.0	Stable at least 15h	[11]
$1Pt/NiAl_2O_4$	210	9.0	2.9	26.5	0.05	26.4	10% loss after 600h	[12]
$0.1\%Pd/ZnAl_2O_4$	250	1.1	0.1	~30	4.5[a]	41.0	-	[13]
Pd/ZnO	250	0.4	0.03	56.3	1.9[a]	-	-	[14]
Pd/Zn0.5Ce	275	1.0	0.1	80.0	20.0[a]	-	Stable at least 50h	[15]
$PdZn/ZnO/Al_2O_3$	350	1.5	0.1	100.0	1.2	-	Stable at least 30h	[16]
5Cd/P25	290	3.0	0.1	100.0	0.07	97.7	Stable at least 150h	This work
		1.0	0.1	92.5	0.2	292.9		

[a] $S_{co} = \frac{n_{co}}{n_{CO}+n_{co_2}} \times 100\%$

Table S10 Assignments of DRIFT spectroscopy peaks corresponding to surface species in the MSR reaction.

Samples	Adsorption peaks (cm^{-1})	Assignment	Species
A R P25	1000~1100; 1300~1500; 2800~3000; 3700~3720	υ (CO); δ_{as} (CH); υ (CH); υ (OH)	Gaseous methanol
	1459	δ_{as} (CH);	Methoxy (*CH_3O) adsorbed on A
	1651	δ (OH)	H_2O adsorbed on A
	1340~1360; 1540~1560; 2860~2870; 2980~2985	υ_s (OCO); υ_{as} (OCO); υ_s (CH); υ_{as} (CH);	Formate (*$HCOO^-$) adsorbed on A, R, and P25
5Cd/A 5Cd/R 5Cd/P25	1335~1345; 1430~1436; 1550~1555; 2800~2830; 2920~2930	δ_s (CH); δ_{as} (CH); υ (OCO); υ_s (CH); υ_{as} (CH)	*CH_3O adsorbed on Cd atoms
	1360~1370; 1530~1545	υ_s (OCO); υ_{as} (OCO)	Monodentate *$HCOO^-$ adsorbed on Cd atoms
	1390~1405; 1590~1600	υ_s (OCO); υ_{as} (OCO)	Bidentate *$HCOO^-$ adsorbed on Cd atoms
	2870~2885; 2950~2980	υ_s (CH); υ_{as} (CH)	*$HCOO^-$ adsorbed on Cd atoms
	2113; 2170	υ (CO)	Gaseous CO
	2308; 2375	υ (CO_2)	Gaseous CO_2

References

1. Jones, S. D. & Hagelin-Weaver, H. E. Steam reforming of methanol over CeO_2- and ZrO_2-promoted Cu-ZnO catalysts supported on nanoparticle Al_2O_3. *Appl. Catal. B* **90**, 195–204 (2009).
2. Li, D. *et al.* Induced activation of the commercial $Cu/ZnO/Al_2O_3$ catalyst for the steam reforming of methanol. *Nat. Catal.* **5**, 99–108 (2022).
3. Wang, L. *et al.* Production of hydrogen by steam reforming of methanol over Cu/ZnO catalysts prepared via a practical soft reactive grinding route based on dry oxalate-precursor synthesis. *J. Catal.* **246**, 193–204 (2007).
4. Liu, Q. *et al.* Waste-free soft reactive grinding synthesis of high-surface-area copper–manganese spinel oxide catalysts highly effective for methanol steam reforming. *Catal. Lett.* **121**, 144–150 (2008).
5. Liu, Y. *et al.* Highly active copper/ceria catalysts for steam reforming of methanol. *Appl. Catal. A* **223**, 137–145 (2002).
6. Jeong, H. *et al.* Hydrogen production by steam reforming of methanol in a micro-channel reactor coated with $Cu/ZnO/ZrO_2/Al_2O_3$ catalyst. *J. Power Sources* **159**, 1296–1299 (2006).
7. Huang, X. The influence of Cr, Zn and Co additives on the performance of skeletal copper catalysts for methanol synthesis and related reactions. *Appl. Catal. A* **257**, 235–243 (2004).
8. Lin, L. *et al.* Low-temperature hydrogen production from water and methanol using Pt/α-MoC catalysts. *Nature* **544**, 80–83 (2017).
9. Cai, F. *et al.* Low-temperature hydrogen production from methanol steam reforming on Zn-modified Pt/MoC catalysts. *Appl. Catal. B* **264**, (2020).
10. Ma, Y. *et al.* Catalytic Activity and stability of nickel-modified molybdenum carbide catalysts for steam reforming of methanol. *J. Phys. Chem. C* **118**, 9485–9496 (2014).
11. Wang, H. *et al.* Titanosilicate zeolite supported Pt nanoparticles with electronic metal-support interactions for efficient methanol steam reforming. *Catal. Today* **382**, 42–47 (2021).
12. Li, D. *et al.* $NiAl_2O_4$ Spinel supported Pt catalyst: High performance and origin in aqueous-phase reforming of methanol. *ACS Catal.* **9**, 9671–9682 (2019).
13. Liu, L. *et al.* $ZnAl_2O_4$ Spinel-Supported $PdZn_\beta$ catalyst with parts per million Pd for methanol steam reforming. *ACS Catal.* **12**, 2714–2721 (2022).
14. Iwasa, N. Mayanagi, T, Masuda, S. & Takezawa, N. Steam reforming of methanol over Pd-Zn Catalysts. *Catal. Lett.* **69**, 355-360 (2000).
15. Barrios, C. E., Bosco, M. V., Baltanás, M. A. & Bonivardi, A. L. Hydrogen production by methanol steam reforming: Catalytic performance of supported-Pd on zinc–cerium oxides' nanocomposites. *Appl. Catal. B* **179**, 262–275 (2015).
16. Yan, P. *et al.* Antioxidative and stable $PdZn/ZnO/Al_2O_3$ catalyst coatings concerning methanol steam reforming for fuel cell-powered vehicles. *Appl. Energy* **268**, 115043 (2020).